

Divergence-Based Adaptive Aggregation for Byzantine Robust Federated Learning

Bingnan Xiao, Feng Zhu, Jingjing Zhang, *Member, IEEE*, Wei Ni, *Fellow, IEEE*, and Xin Wang, *Fellow, IEEE*

Abstract—Inherent client drifts caused by data heterogeneity, as well as vulnerability to Byzantine attacks within the system, hinder effective model training and convergence in federated learning (FL). This paper presents two new frameworks, named DiveRgence-based Adaptive aGgregation (DRAG) and Byzantine-Resilient DRAG (BR-DRAG), to mitigate client drifts and resist attacks while expediting training. DRAG designs a reference direction and a metric named divergence of degree to quantify the deviation of local updates. Accordingly, each worker can align its local update via linear calibration without extra communication cost. BR-DRAG refines DRAG under Byzantine attacks by maintaining a vetted root dataset at the server to produce trusted reference directions. The workers’ updates can be then calibrated to mitigate divergence caused by malicious attacks. We analytically prove that DRAG and BR-DRAG achieve fast convergence for non-convex models under partial worker participation, data heterogeneity, and Byzantine attacks. Experiments validate the effectiveness of DRAG and its superior performance over state-of-the-art methods in handling client drifts, and highlight the robustness of BR-DRAG in maintaining resilience against data heterogeneity and diverse Byzantine attacks.

Index Terms—Federated learning, client drift, Byzantine attack, convergence analysis

I. INTRODUCTION

With the growing complexity of machine learning (ML) tasks and exponential increase in data volumes, federated learning (FL) has received growing attention [1], [2]. Meanwhile, FL with local stochastic gradient descent (SGD) introduces a series of challenges different from centralized learning.

One challenge is client drift due to the lack of persistent communication between workers and the parameter server (PS) [3]. Since the local data of workers can be imbalanced and heterogeneous, i.e., non-independent and identically distributed (non-IID), untimely synchronization of their local updates can cause their models to drift apart [3]. Naively averaging the models, e.g., using Federated Averaging (FedAvg) [1], fails to mitigate such drifts, thwarting convergence.

Another challenge in FL stems from susceptibility to attacks launched by malicious workers due to its distributed nature. These attacks, commonly known as Byzantine attacks [4], [5], disrupt the global model training by tampering with the local

B. Xiao, J. Zhang, and X. Wang are with the Key Laboratory of EMW Information (MoE), College of Future Information Technology, Fudan University, Shanghai 200433, China (e-mail: 22110720061@m.fudan.edu.cn, {jingjingzhang, xwang11}@fudan.edu.cn).

F. Zhu is with the Department of Electrical and Computer Engineering, North Carolina State University, Raleigh, NC, USA. (email: fzhu5@ncsu.edu).

W. Ni is with the School of Engineering, Edith Cowan University, Perth, WA 6027, and the School of Computing Science and Engineering, the University of New South Wales, Sydney, NSW 2052, Australia (e-mail: wei.ni@ieee.org).

data or model updates of the attacked workers, which seriously deteriorate training performance and system security.

A. Related Work

Client drift in FL was first reported in [3], where data heterogeneity can cause local model updates to deviate systematically from the true global gradient direction, thereby introducing bias and impeding convergence. Client drift was further analyzed in [6], [7]. Some works incorporated variance reduction techniques [8] into local SGD, e.g., [9]–[12]. Yet, these methods require full worker participation, limiting their practicality when only partial workers are active.

Another mainstream strategy is to leverage control variates or explicit gradient constraints for update correction. In [13], SCAFFOLD was designed with both local and global control variates to mitigate drifts at the workers. Similarly, FedDyn [14] adopts first-order regularization terms on both the worker and PS sides. MIME [15] utilizes momentum-based gradients to enhance the server-level optimization. As a method based on gradient constraints, FedProx was proposed in [16], which introduced a proximal term into the local objective function to restrict the deviation of local updates from the global model. Built on FedProx, FedDC [17] decouples the local and global models, and integrates both control variates and regularization terms to jointly mitigate the drift between them. FedSAM [18] deploys the SAM optimizer [19], which prompts workers to approximate local flat minima to enhance model generalization. Unfortunately, these approaches incur additional complexity and memory overhead due to the stored control variates and incorporated regularization terms.

Recently, strategies, such as FedExP [20] and FedACG [21], have aimed to improve training convergence by refining the aggregation process. FedExP dynamically adjusts the stepsize at the PS side with extrapolation on pseudo-gradients. FedACG stabilizes training by broadcasting a lookahead global gradient to align the local updates. However, these methods rely on accurate estimation of global or pseudo-gradients, which can be noisy or biased in heterogeneous settings.

On the other hand, FL with local SGD is vulnerable to Byzantine attacks [22]. Common Byzantine attacks include:

- **Noise Injection** [23]: The malicious workers upload random vectors (e.g., sampled from a Gaussian distribution) instead of genuine updates, which corrupt the global model with unpredictable perturbations during training.
- **Sign Flipping** [24]: For the malicious workers, the sign of their local updates is flipped, leading to gradient ascent rather than descent. This actively maximizes the loss and drives the global model away from convergence.

- Label Flipping [25]: This attack erodes local data by reversing each data label l to $L-l-1$, where L is the total number of classes, producing semantically misleading updates while remaining stealthy and API-independent.

Recent works have designed Byzantine-robust aggregation strategies to remove outliers among the workers, i.e., comparing all local updates and suppressing the anomalies [26]–[28]. With techniques, e.g., Krum [26] and Trimmed Mean [27], FL systems can withstand malicious attacks to some extent. In [24], RSA was designed to penalize the difference between local and global model parameters to defend against Byzantine workers. These methods lack robustness against Byzantine attacks when malicious workers become widespread.

In [29], FLTrust was proposed, where the PS leverages a root dataset to guide the global update direction. In [30], the geometric median [31] was adopted for FedAvg due to its strong tolerance against a high proportion of malicious workers. In [32], Byrd-SAGA was developed, which augments the SAGA method [8] with the geometric median to achieve Byzantine robustness. In [33], BROADCAST was proposed, which integrates gradient difference compression with SAGA to mitigate compression and stochastic noise, enhancing resilience to Byzantine attacks. However, these algorithms lack convergence guarantees in Byzantine FL systems with heterogeneous data, particularly for non-convex learning models. Recently, in [34], a convergence guarantee was established for the geometric median under data heterogeneity, albeit relying on the debatable assumption of bounded gradients.

B. Contribution

This paper proposes two new aggregation frameworks, namely DiveRgence-based Adaptive aGgregation (DRAG) and Byzantine-Resilient DRAG (BR-DRAG), to tackle data heterogeneity and malicious Byzantine attacks, and accelerate model training in FL. The key contributions include:

- We interpret client drift as gradient misalignment and define the *degree of divergence* (DoD) to quantify the misalignment between each worker's update and a momentum-based global reference. We propose DRAG to steer local updates toward the reference direction to enhance the alignment in a decentralized manner.
- We strengthen the resistance of DRAG against Byzantine attacks by producing trustworthy reference directions based on a small and vetted root dataset. By aligning and scaling the local updates with the reference direction, this BR-DRAG algorithm mitigates the adverse effect of malicious gradients while preserving their meaningful contribution to aggregations.
- We analyze the convergence of DRAG and BR-DRAG in the non-convex case, accounting for data heterogeneity, partial worker participation, and Byzantine attacks. We reveal that, under both benign and adversarial settings, our algorithms attain the convergence rate of state-of-the-art methods operating without attacks. Also, BR-DRAG sustains convergence while relaxing the conventional assumption on the proportion of malicious workers.

We evaluate the performance of DRAG and BR-DRAG on three broadly adopted datasets: EMNIST, CIFAR-10, and

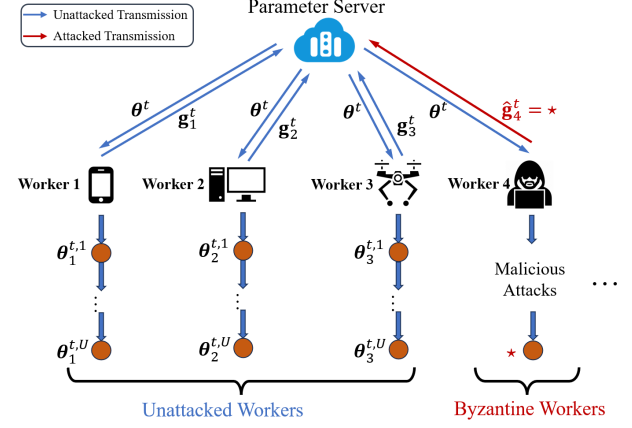


Fig. 1. The architecture of a FL system with S selected workers in round t . For Byzantine FL systems, the attacked workers can upload arbitrary local updates to affect global model aggregation.

CIFAR-100. DRAG effectively mitigates client drifts and accelerates convergence, and consistently outperforms state-of-the-art baselines under heterogeneity and partial worker participation. Under various Byzantine attacks, BR-DRAG shows its superb resilience to severely skewed data distributions and high proportions of malicious workers, compared to existing defense methods, e.g., FLTrust and geometric median.

The rest of this paper is organized as follows. Section II describes the system model. DRAG is developed in Section III, followed by the design of BR-DRAG in Section IV. Section V analyzes the convergence of DRAG and BR-DRAG. Numerical results are provided in Section VI, followed by the conclusions in Section VII.

Notation: Calligraphic letters represent sets; boldface lower-case letters indicate vectors; \mathbb{R} denotes the real number field; $\mathbb{E}[\cdot]$ denotes expectation; ∇ stands for gradient. $\|\cdot\|_2$ is the ℓ_2 -norm; and $\langle \cdot, \cdot \rangle$ represents the inner product operation.

II. SYSTEM MODEL

In this section, we elucidate the FL system and the corresponding setup under Byzantine attacks.

A. Federated Learning Framework

We study an FL system consisting of a PS and M workers collected by the set $\mathcal{M} := \{1, \dots, M\}$; see Fig. 1. Each worker m maintains a local dataset \mathcal{D}_m with N_m data samples. Let $\mathcal{D} = \bigcup_{m \in \mathcal{M}} \mathcal{D}_m$. The objective of FL is to minimize the average sum of local functions of individual workers:

$$\min_{\boldsymbol{\theta} \in \mathbb{R}^d} f(\boldsymbol{\theta}) = \frac{1}{M} \sum_{m=1}^M F_m(\boldsymbol{\theta}), \quad (1)$$

where $\boldsymbol{\theta} \in \mathbb{R}^d$ is the d -dimensional model parameter, and $F_m(\boldsymbol{\theta}) \triangleq \mathbb{E}_{z_m \sim \mathcal{D}_m} [F_m(\boldsymbol{\theta}; z_m)]$ is the smooth local loss function concerning the dataset \mathcal{D}_m of worker m .

With the objective function in (1), we attempt to solve it iteratively using local SGD. In any training round t , the following steps are executed:

- Worker selection and model transmission: The PS first selects a subset $\mathcal{S}^t \subset \mathcal{M}$ with S workers uniformly at

random (UAR) without replacement, and broadcasts the global model θ^t to the selected workers $m \in \mathcal{S}^t$.

- Local update: With $\theta_m^{t,0} = \theta^t$, each selected worker $m \in \mathcal{S}^t$ performs U local updates via SGD updating rule:

$$\theta_m^{t,u+1} = \theta_m^{t,u} - \eta \nabla F_m(\theta_m^{t,u}; z_m^{t,u}), \quad u=0,1,\dots,U-1, \quad (2)$$

where η denotes the stepsize, and $\nabla F_m(\theta_m^{t,u}; z_m^{t,u})$ is the stochastic gradient of worker m with a mini-batch $z_m^{t,u}$ sampled from the local dataset \mathcal{D}_m with size $|z_m^{t,u}| = B$.

- Model uploading and aggregation: After local computation, each worker $m \in \mathcal{S}^t$ sends $\mathbf{g}_m^t = \theta_m^{t,U} - \theta^t$ to the PS, which represents the discrepancy between the latest local model after U local updates and the current global model received at the beginning of the t -th training round. The PS updates the global model θ^{t+1} as

$$\theta^{t+1} = \theta^t + \frac{1}{S} \sum_{m \in \mathcal{S}^t} \mathbf{g}_m^t. \quad (3)$$

Then, the next training round, i.e., the $(t+1)$ -th round, starts. This training process repeats until convergence.

B. Byzantine Attack

Due to the decentralized implementation of FL, workers are vulnerable to Byzantine attacks arising from, e.g., poisoned data. These workers, also known as Byzantine nodes, upload malicious updates to the PS in an attempt to degrade the convergence and learning performance.

Consider A Byzantine nodes out of the M workers. Let \mathcal{A} collect all Byzantine nodes. $\mathcal{A} \subseteq \mathcal{M}$. In the t -th training round, A^t malicious workers, collected by \mathcal{A}^t , are selected, with $\mathcal{A}^t \subseteq \mathcal{S}^t$ and $\mathcal{A}^t \subseteq \mathcal{A}$. Let $w^t \in [0, 1]$ be the intensity level of the Byzantine attack: $A^t = w^t S$.

To launch Byzantine attacks, any malicious worker $m \in A^t$ sends its malicious update $\hat{\mathbf{g}}_m^t \in \mathbb{R}^d$ to the PS. The PS aggregates the local models to update the global model:

$$\theta^{t+1} = \theta^t + \frac{1}{S} \left(\sum_{m \in \mathcal{A}^t} \hat{\mathbf{g}}_m^t + \sum_{m \in \mathcal{B}^t} \mathbf{g}_m^t \right), \quad (4)$$

where $\mathcal{B}^t = \mathcal{S}^t \setminus \mathcal{A}^t$ collects the benign workers in round t .

III. DIVERGENCE-BASED ADAPTIVE AGGREGATION

In this section, we propose the DRAG algorithm, which overcomes client drifts (i.e., the deviation of local model updates from the true global gradient direction, as described in Section I-A) and accelerates convergence. We start with the update flow of DRAG and the overall algorithm.

A. Algorithm Overview

Algorithm 1 presents the implementation details of DRAG based on a new divergence-based aggregation strategy proposed in Section III-C. At the beginning of each training round t , after the worker subset \mathcal{S}^t is specified, the PS determines the *reference direction* \mathbf{r}^t (as proposed in Section III-B), with (5), to measure the degree of local divergence and broadcasts the global model θ^t and the reference direction \mathbf{r}^t to the selected workers; see Steps 4–12.

Algorithm 1 DRAG

- 1: **Input:** $\theta^0, \mathcal{M}, S, T, U, \eta, \alpha, c$;
- 2: **for** $t = 0, 1, \dots, T-1$ **do**
- 3: The PS selects the worker subset $\mathcal{S}^t \subseteq \mathcal{M}$ UAR;
- 4: **if** $t = 0$ **then**
- 5: **for** each worker $m \in \mathcal{S}^t$ in parallel **do**
- 6: Perform U SGD updates by (2), and upload \mathbf{g}_m^t ;
- 7: **end for**
- 8: The PS obtains the reference direction \mathbf{r}^t with (5a);
- 9: **else**
- 10: The PS obtains \mathbf{r}^t with (5b);
- 11: **end if**
- 12: The PS sends θ^t and \mathbf{r}^t to workers $m \in \mathcal{S}^t$
- 13: **for** each worker $m \in \mathcal{S}^t$ in parallel **do**
- 14: Perform U local SGD updates with (2);
- 15: Compute the DoD λ_m^t with (10);
- 16: Compute the modified gradient \mathbf{v}_m^t with (11), and upload \mathbf{v}_m^t to the PS;
- 17: **end for**
- 18: The PS aggregates Δ^t with (6), retains \mathbf{r}^t and Δ^t , and updates θ^t to θ^{t+1} with (7);
- 19: **end for**

On the local side, the workers perform local updates to generate \mathbf{g}_m^t , and compute the DoD λ_m^t , i.e., using (10), to measure the deviation from the reference direction \mathbf{r}^t ; see Steps 14 and 15. To cope with data heterogeneity, the workers generate the modified gradient \mathbf{v}_m^t by adaptively “dragging” their local updates toward \mathbf{r}^t ; see Step 16. After local computation, the selected workers upload $\mathbf{v}_m^t, \forall m \in \mathcal{S}^t$ to the PS for global update. \mathbf{r}^t and Δ^t are retained to construct the reference direction for the next round; see Step 18.

Unlike existing FL systems tackling client drifts by employing local control variates or gradient norms [9]–[18], we design a more effective strategy that guides each local model toward the reference direction through vector manipulation, which enforces directional consistency across clients.

B. Global Reference Direction

As mentioned in Section I, one fundamental challenge in FL is data heterogeneity, as the local gradients $\mathbf{g}_m^t, m \in \mathcal{S}^t$ tend to diverge in direction and magnitude due to discrepancies in the local objective F_m , leading to client drifts and global gradient deviation. Utilizing $\tilde{\Delta}^t = \frac{1}{S} \sum_{m \in \mathcal{S}^t} \mathbf{g}_m^t$ as the global update direction (i.e., using FedAvg, as in conventional FL algorithms) could cause unstable or biased convergence [6].

To address client drifts, we design a global reference direction \mathbf{r}^t produced by the PS at the beginning of each training round t , which helps align the local gradients. At the beginning of training round t , \mathbf{r}^t is constructed as

$$\mathbf{r}^t = \begin{cases} \frac{1}{S} \sum_{m \in \mathcal{S}^t} \mathbf{g}_m^t, & \text{for } t = 0; \\ (1 - \alpha) \mathbf{r}^{t-1} + \alpha \Delta^{t-1}, & \text{for } t \geq 1, \end{cases} \quad (5a)$$

$$\quad (5b)$$

where $\Delta^{t-1} = \frac{1}{S} \sum_{m \in \mathcal{S}^{t-1}} \mathbf{v}_m^{t-1}$ is the aggregated modified gradient in round $t-1$, and $\alpha \in (0, 1)$ is a hyperparameter.

ter controlling the weights of historical reference directions. \mathbf{r}^t , $t \geq 1$, evolves recursively as a weighted combination of the previous reference direction \mathbf{r}^{t-1} and the latest global update Δ^{t-1} .

During round t , the selected devices generate the modified gradients \mathbf{v}_m^t based on the reference direction \mathbf{r}^t (see Section III-C). $\mathbf{v}_m^t, \forall m \in \mathcal{S}^t$, are aggregated at the PS, given as

$$\Delta^t = \frac{1}{S} \sum_{m \in \mathcal{S}^t} \mathbf{v}_m^t. \quad (6)$$

The global model is updated with Δ^t , as given by

$$\boldsymbol{\theta}^{t+1} = \boldsymbol{\theta}^t + \Delta^t. \quad (7)$$

We further derive the closed-form expression of \mathbf{r}^t by deduction, as follows: $\forall t \geq 1$,

$$\mathbf{r}^t = \frac{(1-\alpha)^t}{S} \sum_{m \in \mathcal{S}^0} \mathbf{g}_m^0 + \sum_{i=0}^{t-1} \alpha(1-\alpha)^{t-i-1} \Delta^i. \quad (8)$$

Here, \mathbf{r}^t is an exponential moving average over all historical modified global updates Δ^i , $i = 1, \dots, t-1$, with exponentially decaying weights $(1-\alpha)^{t-i-1}$. This momentum-style construction enables \mathbf{r}^t to preserve long-term memory of update history while prioritizing those more recent. As $\alpha \rightarrow 1$, \mathbf{r}^t reduces to the most recent update Δ^{t-1} . As $\alpha \rightarrow 0$, a smoother reference direction integrates past variations more conservatively. By tuning α , $\mathbf{r}^t, \forall t$, can flexibly balance adaptivity and stability under different data heterogeneity levels.

C. Divergence-based Local Gradient Modification

With the reference direction \mathbf{r}^t , we design the adaptive modified gradients $\mathbf{v}_m^t, \forall m \in \mathcal{S}^t$ per training round t to combat client drifts. We first specify the new metric, DoD, to measure the extent to which the local update \mathbf{g}_m^t of each worker m in round t diverges from \mathbf{r}^t . The angle \angle_m^t is introduced to capture the directional deviation of \mathbf{g}_m^t from \mathbf{r}^t based on the normalized cosine similarity, i.e.,

$$\angle_m^t = \arccos \frac{\langle \mathbf{g}_m^t, \mathbf{r}^t \rangle}{\|\mathbf{g}_m^t\| \cdot \|\mathbf{r}^t\|}, \quad (9)$$

where $\angle_m^t = 0$ indicates perfect alignment, and $\angle_m^t = \pi$ denotes complete opposition. By dividing \angle_m^t over $\frac{\pi}{2}$ and approximating the arccos function with a linear function (e.g., $y = -\frac{\pi}{2}x + \frac{\pi}{2}$), the DoD, λ_m^t , is defined as

$$\lambda_m^t =: c \left(1 - \frac{\langle \mathbf{g}_m^t, \mathbf{r}^t \rangle}{\|\mathbf{g}_m^t\| \cdot \|\mathbf{r}^t\|} \right) \in [0, 2c], \quad (10)$$

where $c \in [0, 1]$ is a tunable hyperparameter modulating the contribution of the divergence signal. By adjusting c , one can control the extent to which local updates are aligned with \mathbf{r}^t . Moreover, λ_m^t quantifies the geometric inconsistency between \mathbf{g}_m^t and \mathbf{r}^t on the unit hypersphere, offering a continuous and differentiable measure of gradient divergence, as opposed to discrete thresholds or binary decisions.

With the reference direction \mathbf{r}^t and the DoD λ_m^t , we establish the modified gradient \mathbf{v}_m^t , which “drags” the local gradients \mathbf{g}_m^t towards \mathbf{r}^t based on λ_m^t , as given by

$$\mathbf{v}_m^t = (1 - \lambda_m^t) \mathbf{g}_m^t + \lambda_m^t \frac{\|\mathbf{g}_m^t\|}{\|\mathbf{r}^t\|} \mathbf{r}^t, \quad (11)$$

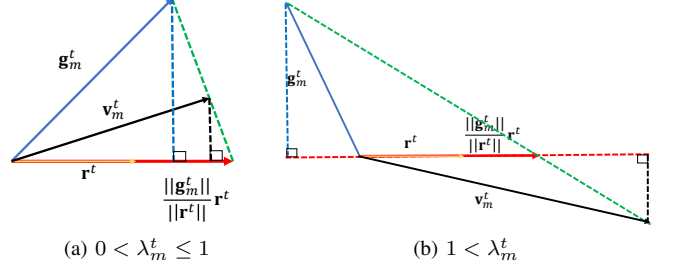


Fig. 2. Illustration of vector modification of DRAG. For workers with different DoD values, the modified gradient \mathbf{v}_m^t (solid black line) has a larger component on the reference direction \mathbf{r}^t (solid yellow line) than the raw local update \mathbf{g}_m^t (solid blue line).

If there is significant misalignment between \mathbf{r}^t and \mathbf{g}_m^t , the local update is dragged toward the normalized reference direction $\frac{\|\mathbf{g}_m^t\|}{\|\mathbf{r}^t\|} \mathbf{r}^t$, reducing client drifts while preserving the diversity of local information.

Fig. 2 illustrates the gradient modification in DRAG based on the proposed reference direction \mathbf{r}^t and DoD λ_m^t . For moderate deviation ($0 < \lambda_m^t \leq 1$) in Fig. 2(a), the modification projects \mathbf{g}_m^t toward \mathbf{r}^t and enlarges the aligned component to at least $\frac{\|\mathbf{g}_m^t\|}{\|\mathbf{r}^t\|} \mathbf{r}^t$, reducing client drifts. For severe deviation ($1 < \lambda_m^t \leq 2$) in Fig. 2(b), the local gradient diverges in the opposite direction to \mathbf{r}^t . We reverse \mathbf{g}_m^t according to (11) to ensure adherence to the correct update direction.

Unlike conventional drift-mitigation methods [13], [14], which rely on local control variates, DRAG aligns local gradients with \mathbf{r}^t via (11), eliminating the need for extra control variables and incurring negligible memory and communication overhead. Moreover, methods employing local gradient-norm regularizers, e.g., [16], are ineffective under heterogeneous data distributions, since local gradients may deviate substantially from the global gradient. In contrast, DRAG attains closer alignment with the global gradient by steering local updates toward \mathbf{r}^t using the DoD metric λ_m^t in (10), accelerating convergence even under severe heterogeneity.

IV. DIVERGENCE-BASED ADAPTIVE AGGREGATION

This section enhances DRAG with resistance to Byzantine attacks, and develops BR-DRAG; see **Algorithm 2**.

A. Algorithm Overview

Unlike DRAG, BR-DRAG maintains a root dataset $\mathcal{D}_{\text{root}}$ for the PS to generate a trusted reference direction before model training. At the beginning of each training round t , the worker subset \mathcal{S}^t is specified. The PS computes the current reference direction \mathbf{r}^t based on $\mathcal{D}_{\text{root}}$ (as opposed to aggregating the local updates $\mathbf{v}_m^t, \forall m \in \mathcal{S}^t$, from the selected workers, as in DRAG), and sends \mathbf{r}^t and the current global model $\boldsymbol{\theta}^t$ to the selected workers; see Step 4.

At the selected workers, either malicious or benign, SGD is performed to generate the local updates $\mathbf{g}_m^t, \forall m \in \mathcal{S}^t$; see Step 6. The selected workers upload \mathbf{v}_m^t to the PS for global update. Based on the DoD, λ_m^t , in (16), the PS compute the modified gradients \mathbf{v}_m^t with (15) to counteract malicious

Algorithm 2 BR-DRAG

- 1: **Input:** $\theta^0, \mathcal{M}, S, T, U, \eta, \alpha, c^t, \mathcal{D}_{\text{root}}$;
- 2: **for** $t = 0, \dots, T - 1$ **do**
- 3: The PS selects $\mathcal{S}^t \subseteq \mathcal{M}$ UAR;
- 4: The PS obtains the reference direction \mathbf{r}^t with (13), and sends θ^t and \mathbf{r}^t to workers $m \in \mathcal{S}^t$;
- 5: **for** each worker $m \in \mathcal{S}^t$ in parallel **do**
- 6: Perform U local SGD updates with (2), and upload \mathbf{g}_m^t to the PS;
- 7: **end for**
- 8: $\forall m \in \mathcal{S}^t$, the PS computes the DoD λ_m^t and modified gradient \mathbf{v}_m^t with (16) and (15);
- 9: The PS updates θ^t to θ^{t+1} with (14);
- 10: **end for**

attacks; see Step 8. The updated global model θ^{t+1} is used to start the next round; see Step 9. Compared to DRAG, BR-DRAG updates both the reference direction \mathbf{r}^t and the module normalization operation to tolerate malicious attacks and ensure system convergence.

B. Byzantine-Resilient Global Reference Direction

To defend against the Byzantine attacks, the key improvements of BR-DRAG over DRAG are the selection of \mathbf{r}^t and the modified gradient \mathbf{v}_m^t .

In the presence of malicious local updates (from the malicious workers), \mathbf{r}^t needs to be constructed in a trustworthy way. Before the training, the PS maintains the small, root dataset $\mathcal{D}_{\text{root}} \subset \mathcal{D}$ to compute \mathbf{r}^t . As assumed in [29], $\mathcal{D}_{\text{root}}$ is trustworthy, e.g., derived from a vetted pool [35] or attested endpoints operating under admission control, employing techniques such as de-duplication and outlier filtering [36]. To hedge against residual interference like label noise, \mathbf{r}^t can be computed via a robust reducer (e.g., trimmed mean [27] or geometric median [31]) over per-sample gradients on $\mathcal{D}_{\text{root}}$.

During training round t , based on $\mathcal{D}_{\text{root}}$, the global model θ^t is updated for U SGD iterations to obtain $\theta^{t,U}$:

$$\theta^{t,u+1} = \theta^{t,u} - \eta \nabla f(\theta^{t,u}; z^{t,u}), \quad u = 0, 1, \dots, U - 1, \quad (12)$$

where $\theta^{t,0} = \theta^t$, and $z^{t,u}$ is drawn independently from $\mathcal{D}_{\text{root}}$ across all batches, local iterations and training rounds.

With $\theta^{t,U}$ obtained from the trusted root dataset $\mathcal{D}_{\text{root}}$, the reference direction \mathbf{r}^t in BR-DRAG is designed as

$$\mathbf{r}^t = \theta^{t,U} - \theta^t = -\eta \sum_{u=0}^{U-1} \nabla f(\theta^{t,u}; z^{t,u}), \quad (13)$$

which, unlike (5) in DRAG, stems directly from $\mathcal{D}_{\text{root}}$, providing a trustworthy update direction of the global objective and thus mitigating the impact of Byzantine behaviors.

The PS aggregates the local updates of the workers as in (4). For each uploaded local update, the PS generates the modified gradient \mathbf{v}_m^t , $\forall m \in \mathcal{S}^t$, to resist Byzantine attacks (as will be designed in Section IV-C). The global model is updated as

$$\theta^{t+1} = \theta^t + \Delta^t = \theta^t + \frac{1}{S} \left(\sum_{m \in \mathcal{A}^t} \hat{\mathbf{v}}_m^t + \sum_{m \in \mathcal{B}^t} \mathbf{v}_m^t \right), \quad (14)$$

where \mathbf{v}_m^t stands for the benign modified gradient (as in DRAG), while $\hat{\mathbf{v}}_m^t$ denotes the malicious modified gradients.

C. Byzantine-Resilient Local Gradient Modification

In FL systems subjected to Byzantine attacks, malicious workers upload distorted gradients resulting from poisoned data. The vector modification in (11) is inapplicable since \mathbf{v}_m^t can be distorted by the unbounded term $(1 - \lambda_m^t) \mathbf{g}_m^t$. To alleviate the impact of malicious local updates on the global model, we design the modified gradient as

$$\mathbf{v}_m^t := (1 - \lambda_m^t) \frac{\|\mathbf{r}^t\|}{\|\mathbf{g}_m^t\|} \mathbf{g}_m^t + \lambda_m^t \mathbf{r}^t, \quad (15)$$

$$\text{with } \lambda_m^t := c^t \left(1 - \frac{\langle \mathbf{g}_m^t, \mathbf{r}^t \rangle}{\|\mathbf{g}_m^t\| \cdot \|\mathbf{r}^t\|} \right) \in [0, 2c^t], \quad (16)$$

where $c^t \in [0, 1]$, $\forall t$ is set to be adjustable across training rounds, as described later in Section V-B.

Unlike DRAG, which modifies the local updates by scaling the reference direction \mathbf{r}^t to match the norm of \mathbf{g}_m^t , i.e., (11), BR-DRAG adopts a different scaling strategy that normalizes \mathbf{g}_m^t to match $\|\mathbf{r}^t\|$; see (15). This modification is essential under Byzantine attacks, where the attackers may inflate the norm of their local updates in an attempt to dominate the aggregation process. By scaling \mathbf{g}_m^t to $\|\mathbf{r}^t\|$, BR-DRAG mitigates the impact of malicious norm. Moreover, with the DoD λ_m^t , BR-DRAG retains the advantages of divergence-based alignment from DRAG, providing directional correction under data heterogeneity. With the reference direction \mathbf{r}^t obtained from a trusted dataset and indicating a general update direction for the training process, as well as the module normalization operation in (15), BR-DRAG can effectively combat the malicious local updates $\hat{\mathbf{g}}_m^t$.

V. CONVERGENCE ANALYSIS OF DRAG AND BR-DRAG

In this section, we establish the convergence rate of DRAG and BR-DRAG for prevalent non-convex objective functions. We start with the following standard assumptions.

Assumption 1. (Smoothness and lower boundedness) Each local objective function $F_m(\theta)$ is L -Lipschitz smooth ($L > 0$):

$$\|\nabla F_m(\theta_1) - \nabla F_m(\theta_2)\| \leq L \|\theta_1 - \theta_2\|, \quad \forall m \in \mathcal{M}. \quad (17)$$

Also, assume the objective function f is lower-bounded by f^* .

Assumption 2. (Unbiasedness and bounded variance) For each client m , the local gradient estimator $\nabla F_m(\theta; z)$ is unbiased, i.e.,

$$\mathbb{E}[\nabla F_m(\theta; z)] = \nabla F_m(\theta), \quad \forall m \in \mathcal{M}. \quad (18)$$

For both the variance of the local gradient estimator and that of the local gradient from the global one, there also exist two constants σ_L^2 and σ_G^2 , such that

$$\mathbb{E}[\|\nabla F_m(\theta; z) - \nabla F_m(\theta)\|^2] \leq \sigma_L^2, \quad \forall m \in \mathcal{M}; \quad (19)$$

$$\mathbb{E}[\|\nabla F_m(\theta) - \nabla f(\theta)\|^2] \leq \sigma_G^2, \quad \forall m \in \mathcal{M}. \quad (20)$$

Assumptions 1 and **2** are standard assumptions considered in non-convex optimization and FL convergence analysis [9]–[18]. Here, σ_G^2 quantifies the degree of data heterogeneity, and $\sigma_G^2 = 0$ indicates IID local data among the workers.

A. Convergence Analysis of DRAG

Under **Assumptions 1** and **2**, we establish the upper bound for the expectation of the average squared gradient norm:

Theorem 1. Suppose that $F_m, \forall m \in \mathcal{M}$ is non-convex, and the stepsize is $\eta \leq \frac{1}{8LU}$. Given an initial model θ^0 , after T training rounds, DRAG guarantees

$$\frac{1}{T} \sum_{t=0}^{T-1} \mathbb{E} [\|\nabla f(\theta^t)\|^2] \leq \frac{f(\theta^0) - f^*}{\gamma \eta UT} + V, \quad (21)$$

where $V = \frac{1}{\gamma \eta U} (c\eta(2\sigma_L^2 + 9\sigma_G^2) + \frac{\eta^2 U^2 L}{2} (\sigma_L^2 + 3U\sigma_G^2) + (\frac{\eta^3 U^2 L^2 (85c+5)}{2} + \frac{15\eta^4 U^3 L^3}{2}) (\sigma_L^2 + 6U\sigma_G^2))$, and $\gamma > 0$.

Proof. See Appendix A. \square

As revealed in **Theorem 1**, DRAG achieves fast convergence for non-convex models under data heterogeneity and partial worker participation. The non-vanishing term V on the RHS of (21) characterizes the effects of both stochastic gradient variance (σ_L^2) and data heterogeneity (σ_G^2) across workers. Meanwhile, the coefficients of σ_L^2 and σ_G^2 increase with the number of local updates, U . To prevent these terms from growing unboundedly as U increases, the stepsize can be set to $\eta = \mathcal{O}(\frac{1}{U})$ to ensure bounded variance accumulation.

In DRAG, the choice of the hyperparameter c in the DoD metric λ_m^t exhibits a trade-off, as setting c too small or too large can adversely impact system performance. A larger c increases λ_m^t in \mathbf{v}_m^t , leading to stronger alignment with the reference direction \mathbf{r}^t , reducing client drifts, as discussed in Section III-C. Several terms in V , e.g., $c\eta(2\sigma_L^2 + 9\sigma_G^2)$, increase linearly with c , reflecting the susceptibility of V to gradient variance under overly aggressive correction.

B. Convergence Analysis of BR-DRAG

Next, we prove the convergence of BR-DRAG. The following assumptions, characterizing the local update properties of the benign workers, are established.

Assumption 3. (Gradient boundedness) For the benign workers, the ratio between the norms of the global reference direction \mathbf{r}^t and the local gradient \mathbf{g}_m^t is bounded, i.e.,

$$\rho_m^t = \frac{\|\mathbf{r}^t\|}{\|\mathbf{g}_m^t\|} \in [p, q], \quad \forall m \in \mathcal{B}^t. \quad (22)$$

where $0 < p < q$ are constants.

Assumption 4. (Bounded divergence) For the benign workers, define the cosine similarities $y_m^t = \frac{\langle \mathbf{g}_m^t, \mathbf{r}^t \rangle}{\|\mathbf{g}_m^t\| \|\mathbf{r}^t\|}$. The weighted aggregations of y_m^t is bounded, $\forall t$, i.e.,

$$\rho^t = \frac{1}{S} \sum_{m \in \mathcal{B}^t} y_m^t \rho_m^t \in [0, (1 - w^t)q]; \quad (23)$$

where $w^t \in [0, 1]$ denotes the intensity level of the Byzantine attack defined in Section II-B.

Unlike the typical bounded gradient assumptions, e.g., [6, Asm. 4] and [34, Asm. 5], **Assumption 3** only requires a bounded ratio between the trusted reference direction \mathbf{r}^t and the benign local gradients $\mathbf{g}_m^t, \forall m$, without restricting their

individual magnitudes, relaxing constraints on modeling data heterogeneity, and accommodating diverse data distributions, compared to the typical requirement of uniform gradient norms (i.e., $\|\mathbf{g}_m^t\| \leq G$ [6], [34]). This relaxation better reflects practical federated settings with non-IID data.

In **Assumption 4**, (23) enforces that the weighted average of the cosine similarities between the benign workers' gradients and trusted reference direction \mathbf{r}^t , scaled by their gradient-norm ratios ρ_m^t , remains within $[0, (1 - w^t)q]$. In other words, the benign updates are assumed to be positively aligned with \mathbf{r}^t and have bounded relative magnitudes. The benign contribution to the aggregation maintains a consistent descent direction without being dominated by excessively large updates.

Interestingly, we do not assume explicit bounds or range for the cosine similarities of the malicious workers $m \in \mathcal{A}^t$. The only assumption about the Byzantine attacks is the intensity level of attacks, i.e., w^t in (23). This substantially relaxes the reliance of our analysis and findings on assumptions of a-priori knowledge about the system.

Under **Assumptions 1–4**, the following theorem establishes.

Theorem 2. Suppose that $F_m, \forall m \in \mathcal{M}$ is non-convex. Given an initial model θ^0 , after T training rounds,

- if $c^t = \frac{w^t}{w^t - x^t} \in [\frac{1}{2}, 1]$ and the stepsize satisfies $\eta \leq \frac{(1-\tilde{w})(1-\tilde{c})p}{32U+2UL^2(p+2q^2)}$, BR-DRAG guarantees

$$\frac{1}{T} \sum_{t=0}^{T-1} \mathbb{E} [\|\nabla f(\theta^t)\|^2] \leq \frac{f(\theta^0) - f^*}{\chi \eta UT} + W, \quad (24)$$

where $\chi > 0$, $\tilde{c} = \max_t \frac{w^t}{w^t - x^t}$, $\tilde{w} = \max_t w^t$, and $W = \frac{2\eta\sigma_L^2}{\chi} \left(\frac{(1+\tilde{w})\tilde{c}\eta UL^2}{2} + \frac{\eta UL^2 q^2}{2(1-\tilde{c})p} + 1 \right)$.

- if η and c^t satisfy $\eta \leq \frac{2c^t(1-c^t)(1-w^t)(1-w^t-y^t)p}{32pU+c^tUL^2(p^2+q^2)}$ and $((p^t)^2 - 7w^t + 8x^t - 1) (c^t)^2 + (15w^t + 1)c^t \geq \frac{8(w^t)^2}{w^t - x^t}$, $\forall t$, respectively, BR-DRAG guarantees

$$\frac{1}{T} \sum_{t=0}^{T-1} \mathbb{E} [\|\nabla f(\theta^t)\|^2] \leq \frac{f(\theta^0) - f^*}{\chi \eta UT} + W, \quad (25)$$

where $\chi > 0$, $\tilde{c} = \max_t c^t$, $\tilde{w} = \max_t w^t$, $x^t = \frac{1}{S} \sum_{m \in \mathcal{A}^t} x_m^t$ with $x_m^t = \frac{\langle \mathbf{g}_m^t, \mathbf{r}^t \rangle}{\|\mathbf{g}_m^t\| \|\mathbf{r}^t\|}$, $y^t = \frac{1}{S} \sum_{m \in \mathcal{B}^t} y_m^t$, and $W = \frac{2\eta\sigma_L^2}{\chi} \left(\frac{(1+\tilde{w})\tilde{c}\eta UL^2}{2} + \frac{\eta UL^2 q^2}{2(1-\tilde{c})p} + H + 1 \right)$ with $H = \max_t \frac{\|w^t(1-c^t) + c^t x^t\|}{2c^t \eta U (w^t - x^t)}$.

Proof. See Appendix B. \square

According to **Theorem 2**, BR-DRAG converges under Byzantine attacks in the presence of heterogeneity and partial aggregation, unlike conventional methods, e.g., [24], [26], [27]. The constant W specifies the non-vanishing error caused by gradient variance, data heterogeneity, and adversarial attacks. In each training round t , the malicious updates induce the increased errors $\delta^t = c^t(w^t - x^t)\eta U$ and $\kappa^t = c^t(1-w^t-y^t)\eta U$ in (47), impeding convergence. Based on (15), BR-DRAG projects the malicious vectors on a bounded space \mathbf{r}^t , i.e., the trusted reference direction, tolerating the malicious updates.

The resistance of BR-DRAG to malicious worker participation is achieved by reducing the stepsize η and enhancing

the gradient alignment degree. As the proportion of malicious workers increases (i.e., w^t grows), the hyperparameter c^t needs to increase, which in turn reduces the effective stepsize. This adjustment slows convergence to maintain the conditions necessary for stability and robustness. An excessively large c^t amplifies the variance-related components, e.g., $\frac{\tilde{c}(1+\tilde{w})L^2}{\chi}\eta^2U\sigma_L^2$ in W in BR-DRAG, while an excessively small c^t may degrade gradient alignment in (15), heightening the vulnerability to adversarial gradients. To this end, c^t should be calibrated meticulously to suppress adversarial deviation while controlling gradient variance in BR-DRAG.

Unlike a majority of the existing Byzantine-resilient FL algorithms [24], [29], [30], [32]–[34], which typically require the condition of $A^t < \frac{S}{2}, \forall t$, BR-DRAG allows an arbitrary proportion of malicious workers in each round. This is enabled by the design of the reference direction in (13) and gradient modification in (15), suppressing the effects of malicious gradient aggregation. Moreover, by plugging $\eta = \mathcal{O}(\frac{1}{\sqrt{T}})$ and $U = \mathcal{O}(1)$ into (25), BR-DRAG maintains the same convergence rate of $\mathcal{O}(\frac{1}{\sqrt{T}})$ as DRAG, which is consistent with FL algorithms without Byzantine attacks [16].

VI. EXPERIMENTS AND RESULTS

This section experimentally evaluates DRAG and BR-DRAG compared to state-of-the-art FL and Byzantine-resilient FL algorithms, with the following datasets and models:

- EMNIST dataset [37]: For the digit and letter classification task, we utilize the “balanced” data split containing 131,600 samples with 47 classes. The designed Convolutional Neural Network (CNN) comprises two 5×5 convolutional layers and two fully connected layers, with a final output layer for 47-class classification.
- CIFAR-10 dataset [38]: For the image classification task, the CIFAR-10 dataset is composed of 60,000 color images in a total of 10 classes. We employ a CNN with two 5×5 padded convolutional layers to extract hierarchical features and predict across 10 classes.
- CIFAR-100 dataset [38]: For the fine-grained image classification task, the CIFAR-100 dataset contains 60,000 color images categorized into 100 classes. We adopt a deeper CNN comprising three 3×3 padded convolutional layers followed by max pooling operations, and two fully connected layers, culminating in a 100-class output layer.

Consider an FL system with 40 workers, and each worker performs $U = 5$ local updates in each training round. To characterize data heterogeneity, we utilize the Dirichlet distribution with parameter β [18], [20], [21]. Specifically, we sample $p_k \sim \text{Dir}(\beta)$ and allocate a proportion $p_{k,j}$ of image class k instances to device j . A smaller β represents a more imbalanced data distribution. Here, we choose $\beta = 0.1$ and 0.5 to represent strong and moderate data heterogeneity, respectively. By default, we set the stepsize $\eta = 0.01$ and the batch size is 10. To simulate partial worker participation, we set the worker subset size to $S = 10$ per round. The FL environment is set up in PyTorch 2.5.1 on a Windows 10 operating system with one 4090 GPU.

A. Evaluation of DRAG

We first compare DRAG with the following benchmarks, which have been successfully deployed in FL systems.

- FedAvg [1]: The local and global models are updated as (2) and (3), respectively.
- FedProx [16]: In any training round t , the workers perform U local updates with a regularization term to approximate a γ -inexact solution: $\|\nabla F_m(\theta_m^{t,u}) + \mu(\theta_m^{t,u} - \theta^t)\| \leq \gamma \|\nabla F_m(\theta^t)\|$.
- SCAFFOLD [13]: In any training round t , the local update is employed with control variates: $\theta_m^{t,u} = \theta_m^{t,u} - \eta(\nabla F_m(\theta_m^{t,u}; z_m^{t,u}) - h_m^t + h^t)$, where h_m^t and h^t are updated as $h_m^{t+1} = \nabla F_m(\theta^t; z_m^{t,0})$ and $h^{t+1} = h^t + \frac{1}{M} \sum_{i \in \mathcal{S}^t} (\nabla F_m(\theta^t; z_m^{t,0}) - h_m^t)$.
- FedExP [20]: With $\Delta^t = \frac{1}{S} \sum_{i \in \mathcal{S}^t} \mathbf{g}_m^t$ and a small positive constant ϵ , the global model is updated as $\theta^{t+1} = \theta^t + \frac{\eta_g^t}{S} \sum_{m \in \mathcal{S}^t} \mathbf{g}_m^t$, where $\eta_g^t = \max \left\{ 1, \frac{\sum_{i \in \mathcal{S}^t} \|\mathbf{g}_m^t\|^2}{2S(\|\Delta^t\|^2 + \epsilon)} \right\}$.
- FedACG [21]: The local updates are performed as $\theta_m^{t,u+1} = \theta_m^{t,u} - \eta(\nabla F_m(\theta_m^{t,u}; z_m^{t,u}) + \beta \|\theta_m^{t,u} - (\theta^{t-1} + \lambda m^{t-1})\|)$ with the lookahead gradient updated as $m^t = \lambda m^{t-1} + \frac{1}{S} \sum_{m \in \mathcal{S}^t} \mathbf{g}_m^t$.

After fine-tuning these benchmarks, we set $\mu = 0.2$ for FedProx; $\epsilon = 0.001$ for FedExP; $\beta = 0.2$ and $\lambda = 0.85$ for FedACG. For DRAG, $\alpha = 0.25$, $c = 0.1$ for moderate data heterogeneity, and $c = 0.25$ for strong data heterogeneity.

Figs. 3 to 5 show the convergence of the algorithms. Across different datasets and data heterogeneity levels, DRAG significantly outperforms the benchmarks, validating **Theorem 1**. The accuracy gap between DRAG and FedAvg is larger when data heterogeneity is more severe (from $\beta = 0.5$ to $\beta = 0.1$), confirming the effective client-drift mitigation of DRAG. Meanwhile, DRAG converges considerably faster than the benchmarks, and achieves 70% test accuracy within 600 rounds in Fig. 4(b). Over 1,400 rounds are needed for other algorithms, e.g., SCAFFOLD and FedExP, verifying that the adaptive aggregation of DRAG in (11) accelerates the decrease in the global loss function.

FedProx demonstrates subpar performance due to the lack of enough local computations to achieve the required γ -inexact solution. With the additional lookahead gradient, FedACG achieves a limited accuracy improvement over FedProx. FedExP is limited by the later stage of training and degrades to FedAvg. Since the control variate $\nabla F_m(\theta^t) - \mathbb{E}[h_m^t] + \mathbb{E}[h^t] \neq 0$ when $\theta^t = \theta^*$, the local models of SCAFFOLD deviate from θ^* and necessitate additional training rounds to mitigate this imbalance of control variate. By balancing the local gradient direction and the reference direction, DRAG avoids using control variates or regularization terms, realizing adaptive model training without additional communication overhead.

Fig. 6 evaluates DRAG under different numbers of participating workers, where a UAR selection of $S = 5, 15, 25$, and 35 out of $M = 40$ workers is considered. Clearly, more worker participation leads to faster convergence under both data distributions. A larger number of selected workers S contributes to more stable reference directions $\mathbf{r}^t, \forall t$, in (8) and helps better guide local gradient modifications.

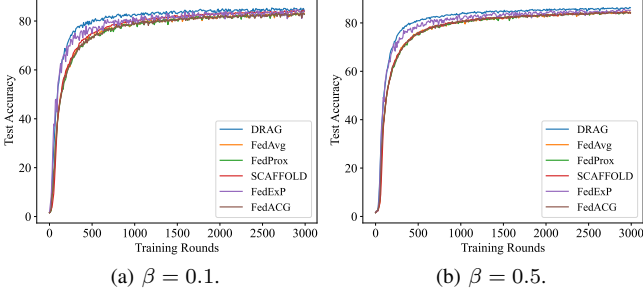


Fig. 3. Convergence performance of different algorithms on EMNIST.

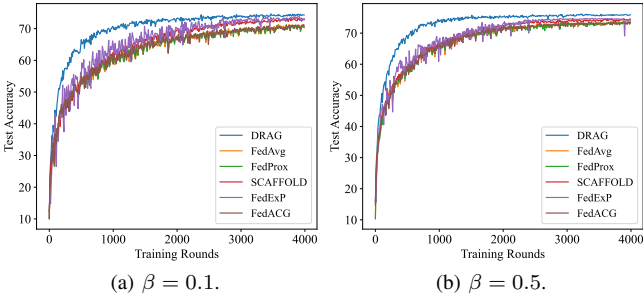


Fig. 4. Convergence performance of different algorithms on CIFAR-10.

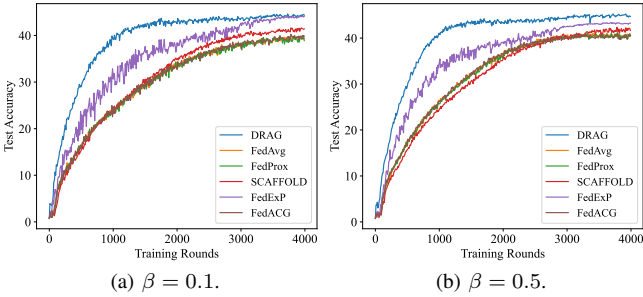


Fig. 5. Convergence performance of different algorithms on CIFAR-100.

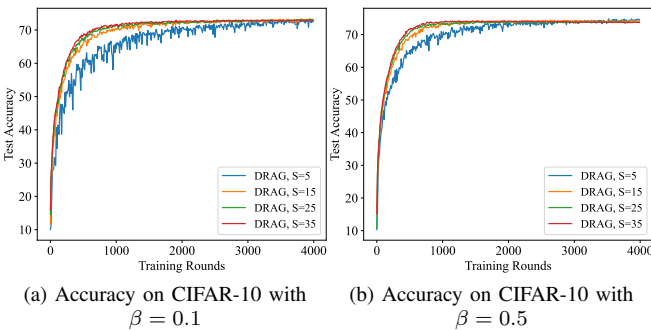


Fig. 6. Convergence performance of DRAG with different numbers of participating workers on CIFAR-10.

Figs. 7 and 8 examine the impact of the hyperparameters α and c in (8) and (10) on the performance of DRAG. Fig. 7(a) demonstrates an overly small $\alpha = 0.01$ in (8) overuses historical gradients, where unstable gradients in the early training stage hinder convergence. When α is large, e.g., $\alpha > 0.25$, the reference direction \mathbf{r}^t depends excessively on Δ^{t-1} , making

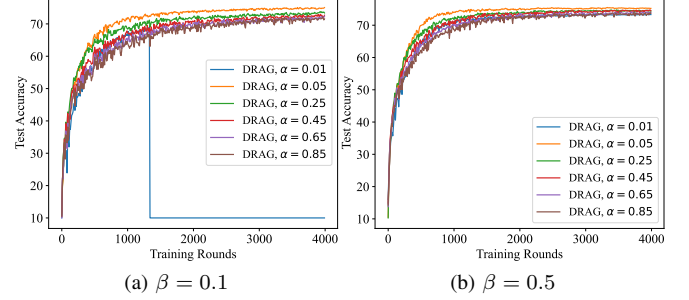


Fig. 7. Convergence performance of DRAG with different values of hyperparameter α on CIFAR-10.

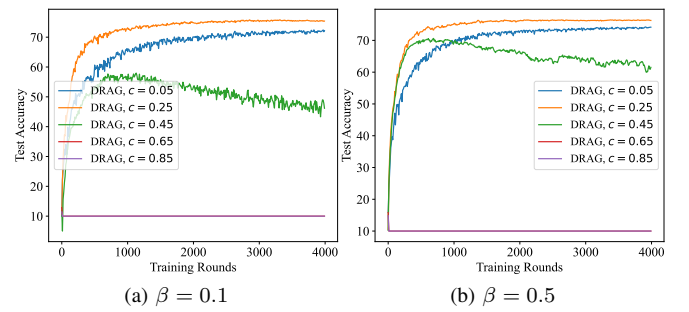


Fig. 8. Convergence performance of DRAG with different values of hyperparameter c on CIFAR-10.

it difficult to find a fast descent path. In Fig. 7(b), although the data heterogeneity becomes moderate, an overly large or small value of α slows down the convergence. Fig. 8 shows that too large or too small c significantly impairs training, since it would penalize gradient variance control or gradient alignment. This is consistent with the analysis in Section V-B, confirming the importance of careful configuration of c .

B. Evaluation of BR-DRAG

We proceed to evaluate the BR-DRAG framework under Byzantine attacks by considering the following benchmarks.

- FedAvg [1]: The local and global models are updated following (2) and (4), respectively.
- FLTrust [29]: In any training round t , the local gradients are modified with ReLU-clipped cosine similarity: $\tilde{\mathbf{g}}_m^t = \max(0, \cos(\mathbf{g}_m^t, \mathbf{r}^t)) \|\mathbf{g}_m^t\| \frac{\mathbf{r}^t}{\|\mathbf{r}^t\|}$, where \mathbf{r}^t is the reference direction designed in a similar way to (13).
- RFA [30]: The global model is updated via geometric median aggregation: $\theta^{t+1} = \text{GeoMed}(\{\theta_m^{t,U}\}_{m \in \mathcal{S}^t})$, where $\text{GeoMed}(\cdot)$ minimizes the sum of distances to all local models and is solved with the Weiszfeld algorithm [39].
- RAGA [34]: The global gradient \mathbf{g}^t is acquired with the geometric median metric: $\mathbf{g}^t = \text{GeoMed}(\{\mathbf{g}_m^t\}_{m \in \mathcal{S}^t})$, and the global model is updated as $\theta^{t+1} = \theta^t + \mathbf{g}^t$.

For malicious workers, we deploy three different attack methods, including noise injection [23], sign flipping [24], and label flipping [25]; see Section I-B. For the noise injection attack, we set malicious local gradients to $p_m^t \mathbf{g}_m^t, \forall m \in \mathcal{A}^t$, where p_m^t conforms to the Gaussian distribution $\mathcal{N}(0, 3)$. For the sign flipping attack, the malicious workers generate $-\mathbf{g}_m^t, \forall m \in \mathcal{A}^t$

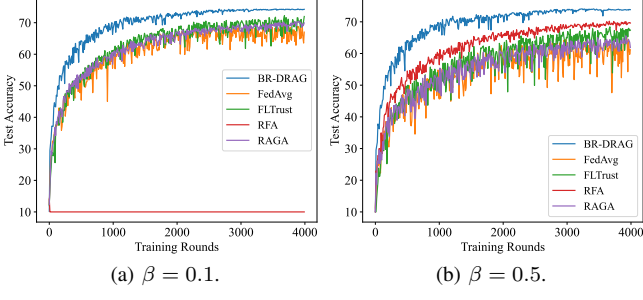


Fig. 9. Convergence performance of different algorithms on CIFAR-10 under the noise injection attack.

as the local gradient. For the label flipping attack, half of local data labels of the malicious workers are reversed. Under BR-DRAG, $c^t = 0.5, \forall t$, and $\mathcal{D}_{\text{root}}$ is constructed with 3,000 data samples drawn randomly and uniformly in equal proportions from trusted workers; see Section IV-B.

We set the ratio of malicious workers to $\frac{A}{M} = 30\%$ in the system. Figs. 9 to 14 evaluate the training performance of BR-DRAG under the different Byzantine attack methods, datasets, and data heterogeneity levels. Compared to the benchmarks, BR-DRAG demonstrates superior adaptability and robustness against severe data heterogeneity and attacks, validating **Theorem 2**. For example, BR-DRAG surpasses FLTrust in accuracy by 13.4% and 9.8% in Figs. 11(a) and 11(b), respectively. Based on (15) and using a larger c than DRAG, BR-DRAG effectively suppresses malicious gradients while amplifying the impact of benign updates.

On the other hand, no benchmarks maintain stability under the diverse Byzantine attacks. RFA and RAGA can approach BR-DRAG in performance since the applied Weiszfeld algorithm can resist the interference of extreme gradient values. The ReLU-clipping design in FLTrust lacks fine-grained control, as it would entirely preclude the attackers or workers with excessively biased local data. In contrast, a key advantage of BR-DRAG is that it retains only the directionally consistent component of each received update with respect to \mathbf{r}^t , and suppresses misalignment. As shown in Figs. 15 to 17, even when the proportion of Byzantine workers increases to $\frac{A}{M} = 60\%$, BR-DRAG maintains convergence. This surpasses all benchmarks, which typically require $\frac{A}{M} < 50\%$, validating the analysis in Section V-C. The benchmarks based on the geometric median, i.e., RFA and RAGA, suffer severe degradation, as the high proportion of malicious workers significantly distorts the centroid estimation. In contrast, BR-DRAG converges by regulating the magnitude and direction of malicious updates, demonstrating its distinctive robustness under high data heterogeneity and severe Byzantine attacks.

VII. CONCLUSION AND FUTURE WORK

In this paper, we designed DRAG to address client drifts caused by data heterogeneity in FL systems. With the proposed reference direction and DoD, the local updates can be adaptively dragged towards the global update direction. We further developed BR-DRAG, a Byzantine-resilient variant of

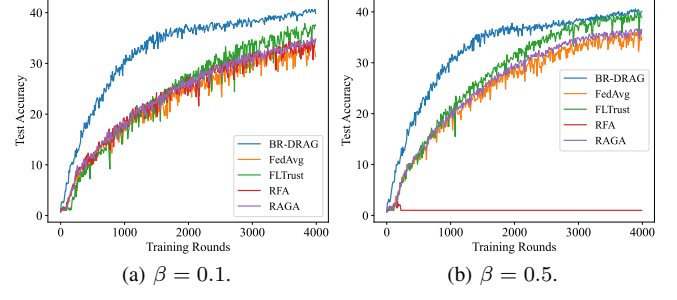


Fig. 10. Convergence performance of different algorithms on CIFAR-100 under the noise injection attack.

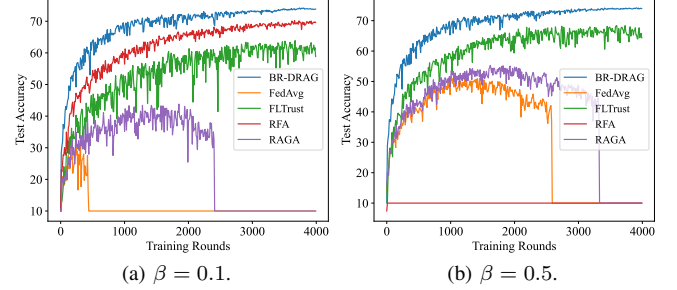


Fig. 11. Convergence performance of different algorithms on CIFAR-10 under the sign flipping attack.

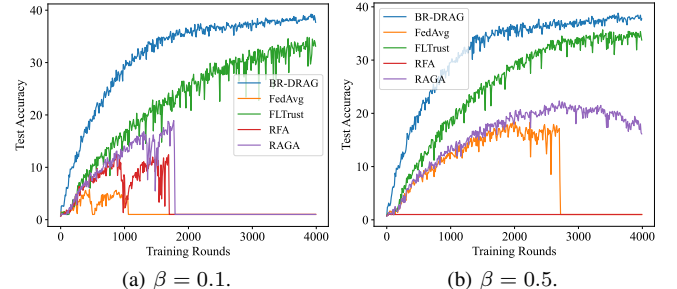


Fig. 12. Convergence performance of different algorithms on CIFAR-100 under the sign flipping attack.

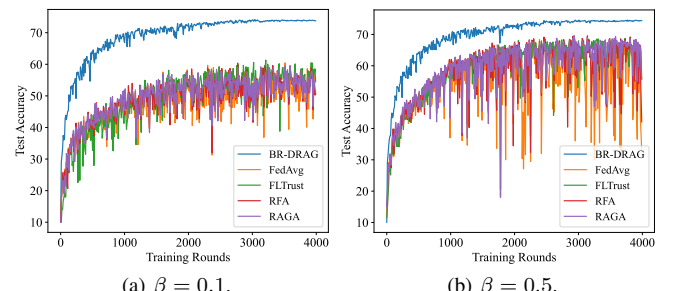


Fig. 13. Convergence performance of different algorithms on CIFAR-10 under the label flipping attack.

DRAG, to resist Byzantine attacks. Comprehensive convergence analyses of DRAG and BR-DRAG with non-convex loss functions were conducted under data heterogeneity, partial worker participation, and Byzantine attacks. It was revealed that both DRAG and BR-DRAG achieve fast convergence

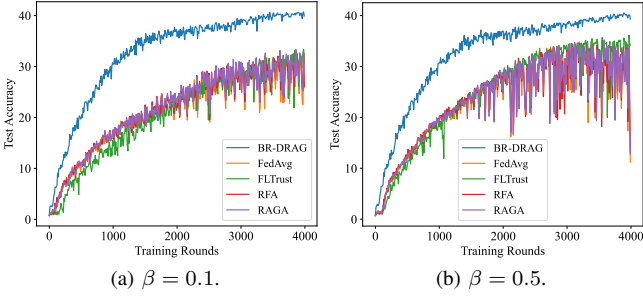


Fig. 14. Convergence performance of different algorithms on CIFAR-100 under the label flipping attack.

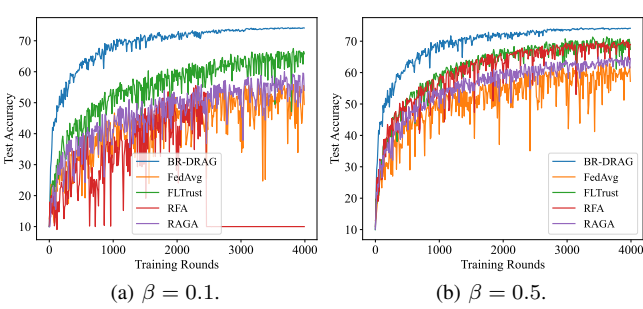


Fig. 15. Convergence performance of different algorithms on CIFAR-10 under the noise injection attack, where 60% of the workers are attackers.

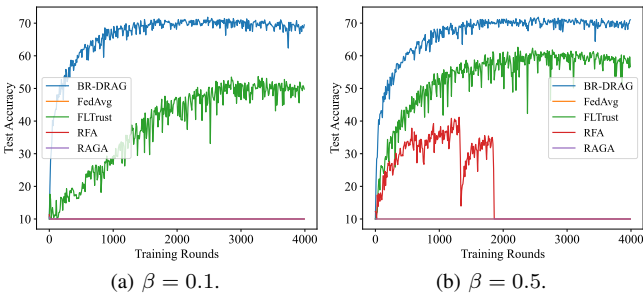


Fig. 16. Convergence performance of different algorithms on CIFAR-10 under the sign flipping attack, where 60% of the workers in the system are attackers.

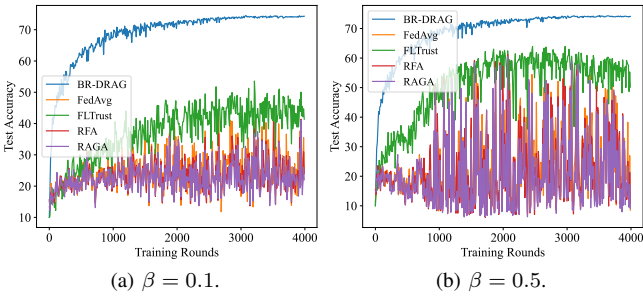


Fig. 17. Convergence performance of different algorithms on CIFAR-10 under the label flipping attack, where 60% of the workers in the system are attackers.

compared to the existing algorithms. Numerical results validated the superiority of DRAG in mitigating data heterogeneity and accelerating model convergence, and the robustness of BR-DRAG against malicious attacks. In the future, we will extend DRAG and BR-DRAG to decentralized FL settings.

APPENDIX A PROOF OF THEOREM 1

Based on the L -smoothness of f , we first have:

$$\begin{aligned} \mathbb{E}[f(\boldsymbol{\theta}^{t+1})] &\leq f(\boldsymbol{\theta}^t) + \langle \nabla f(\boldsymbol{\theta}^t), \mathbb{E}[\boldsymbol{\theta}^{t+1} - \boldsymbol{\theta}^t] \rangle + \frac{L}{2} \mathbb{E}[\|\boldsymbol{\theta}^{t+1} - \boldsymbol{\theta}^t\|^2] \\ &= f(\boldsymbol{\theta}^t) + \langle \nabla f(\boldsymbol{\theta}^t), \mathbb{E}[\Delta^t + a_1 - a_1] \rangle + \frac{L}{2} \mathbb{E}[\|\Delta^t\|^2] \\ &\stackrel{(a)}{=} f(\boldsymbol{\theta}^t) - (1-c)\eta U \mathbb{E}[\|\nabla f(\boldsymbol{\theta}^t)\|^2] + \frac{L}{2} T_1 + T_2, \end{aligned} \quad (26)$$

where $\Delta^t = \boldsymbol{\theta}^{t+1} - \boldsymbol{\theta}^t$, and $a_1 = (1-c)\eta U \nabla f(\boldsymbol{\theta}^t)$; (a) is due to $T_1 = \mathbb{E}[\|\Delta^t\|^2]$ and $T_2 = \langle \nabla f(\boldsymbol{\theta}^t), \mathbb{E}[\Delta^t + a_1] \rangle$.

Next, we bound T_1 and T_2 . For T_1 , we have

$$\begin{aligned} T_1 &= \mathbb{E} \left[\left\| \frac{1}{S} \sum_{m \in \mathcal{S}^t} \left((1 - \lambda_m^t) \mathbf{g}_m^t + \frac{\lambda_m^t \|\mathbf{g}_m^t\| \mathbf{r}^t}{\|\mathbf{r}^t\|} \right) \right\|^2 \right] \\ &\stackrel{(a)}{\leq} \mathbb{E} \left[\left(\frac{1}{S} \sum_{m \in \mathcal{S}^t} \left((1 - \lambda_m^t) \|\mathbf{g}_m^t\| + \frac{\lambda_m^t \|\mathbf{g}_m^t\| \|\mathbf{r}^t\|}{\|\mathbf{r}^t\|} \right) \right)^2 \right] \\ &\stackrel{(b)}{\leq} \frac{\eta^2}{S} \sum_{m \in \mathcal{S}^t} \mathbb{E} \left[\left\| \sum_{u=0}^{U-1} \nabla F(\boldsymbol{\theta}_m^{t,u}; z_m^{t,u}) \right\|^2 \right] \\ &\stackrel{(c)}{=} \frac{\eta^2}{S} \sum_{m \in \mathcal{S}^t} \left(\mathbb{E} \left[\left\| \sum_{u=0}^{U-1} a_2 \right\|^2 \right] + \mathbb{E} \left[\left\| \sum_{u=0}^{U-1} \nabla F_m(\boldsymbol{\theta}_m^{t,u}) \right\|^2 \right] \right) \\ &\stackrel{(d)}{=} \eta^2 U \sigma_L^2 + \frac{\eta^2}{M} \sum_{m \in \mathcal{M}} \mathbb{E} \left[\left\| \sum_{u=0}^{U-1} \nabla F_m(\boldsymbol{\theta}_m^{t,u}) \right\|^2 \right], \end{aligned} \quad (27)$$

where $a_2 = \nabla F_m(\boldsymbol{\theta}_m^{t,u}; z_{m,b}^{t,u}) - \nabla F_m(\boldsymbol{\theta}_m^{t,u})$; (a) is due to the triangle inequality; (b) is based on the definition of \mathbf{g}_m^t and Cauchy-Schwartz inequality; (c) follows from $\mathbb{E}[\|\mathbf{x}\|^2] = \mathbb{E}[\|\mathbf{x} - \mathbb{E}[\mathbf{x}]\|^2 + \|\mathbb{E}[\mathbf{x}]\|^2]$ and **Assumption 2**; (d) comes from $\mathbb{E}[\|\mathbf{x}_1 + \dots + \mathbf{x}_n\|^2] = \mathbb{E}[\|\mathbf{x}_1\|^2 + \dots + \|\mathbf{x}_n\|^2]$ if \mathbf{x}_i , $\forall i$, is zero-mean and independent, **Assumption 2**, and UAR worker sampling.

We can rewrite T_2 as

$$\begin{aligned} T_2 &\stackrel{(a)}{=} \left\langle \nabla f(\boldsymbol{\theta}^t), \mathbb{E} \left[(1-c) \mathbf{g}^t + \frac{c}{S} \sum_{m \in \mathcal{S}^t} \frac{\langle \mathbf{g}_m^t, \mathbf{r}^t \rangle}{\|\mathbf{g}_m^t\| \|\mathbf{r}^t\|} \mathbf{g}_m^t \right. \right. \\ &\quad \left. \left. + \frac{c}{S} \sum_{m \in \mathcal{S}^t} \frac{\|\mathbf{g}_m^t\| \|\mathbf{r}^t\| - \langle \mathbf{g}_m^t, \mathbf{r}^t \rangle}{\|\mathbf{r}^t\|^2} \mathbf{r}^t + (1-c)\eta U \nabla f(\boldsymbol{\theta}^t) \right] \right\rangle \\ &\stackrel{(b)}{=} \underbrace{\left\langle \nabla f(\boldsymbol{\theta}^t), \mathbb{E}[(1-c)\mathbf{g}^t + a_1] \right\rangle}_{T_{2,1}} + T_{2,2} + T_{2,3}, \end{aligned} \quad (28)$$

where $T_{2,2} = \langle \nabla f(\boldsymbol{\theta}^t), \mathbb{E}[\frac{c}{M} \sum_{m \in \mathcal{S}^t} \frac{\langle \mathbf{g}_m^t, \mathbf{r}^t \rangle}{\|\mathbf{g}_m^t\| \|\mathbf{r}^t\|} \mathbf{g}_m^t] \rangle$, and $T_{2,3} = \langle \nabla f(\boldsymbol{\theta}^t), \mathbb{E}[\frac{c}{M} \sum_{m \in \mathcal{S}^t} \frac{\|\mathbf{g}_m^t\| \|\mathbf{r}^t\| - \langle \mathbf{g}_m^t, \mathbf{r}^t \rangle}{\|\mathbf{r}^t\|^2} \mathbf{r}^t] \rangle$; (a) is based on the definition of Δ^t , and (b) comes from decomposition of $\mathbf{g}^t = \frac{1}{S} \sum_{m \in \mathcal{S}^t} \mathbf{g}_m^t$.

We proceed to bound $T_{2,1}$, $T_{2,2}$ and $T_{2,3}$ in (28). The upper bound of $T_{2,1}$ is given by

$$\begin{aligned} T_{2,1} &\stackrel{(a)}{=} \left\langle \nabla f(\boldsymbol{\theta}^t), \mathbb{E}[(1-c)\bar{\mathbf{g}}^t + a_1] \right\rangle \\ &\stackrel{(b)}{=} \left\langle \nabla f(\boldsymbol{\theta}^t), \mathbb{E} \left[- (1-c) \frac{1}{M} \sum_{m \in \mathcal{M}} \sum_{u=0}^{U-1} \eta \nabla F_m(\boldsymbol{\theta}_m^{t,u}) \right. \right. \\ &\quad \left. \left. + (1-c)\eta U \frac{1}{M} \sum_{m \in \mathcal{M}} \nabla F_m(\boldsymbol{\theta}^t) \right] \right\rangle \end{aligned}$$

$$\begin{aligned}
&= \left\langle \sqrt{\eta U(1-c)} \nabla f(\boldsymbol{\theta}^t), -\frac{\sqrt{\eta(1-c)}}{M\sqrt{U}} \mathbb{E} \left[\sum_{m \in \mathcal{M}} \sum_{u=0}^{U-1} a_3 \right] \right\rangle \\
&\stackrel{(c)}{\leq} a_4 + \frac{(1-c)\eta}{2UM^2} \mathbb{E} \left[\left\| \sum_{m \in \mathcal{M}} \sum_{u=0}^{U-1} a_3 \right\|^2 \right] \\
&\stackrel{(d)}{\leq} a_4 + \frac{(1-c)\eta L^2}{2M} \sum_{m \in \mathcal{M}} \sum_{u=0}^{U-1} \mathbb{E} \left[\|\boldsymbol{\theta}_m^{t,u} - \boldsymbol{\theta}^t\|^2 \right], \quad (29)
\end{aligned}$$

where $\bar{\mathbf{g}}^t = \frac{1}{M} \sum_{m \in \mathcal{M}} \mathbf{g}_m^t$, $a_3 = \nabla F_m(\boldsymbol{\theta}_m^{t,u}) - \nabla F_m(\boldsymbol{\theta}^t)$, and $a_4 = \frac{(1-c)\eta U}{2} \mathbb{E} [\|\nabla f(\boldsymbol{\theta}^t)\|^2]$; (a) is due to identical sampling distribution in each round; (b) comes from the definition of $\bar{\mathbf{g}}^t$; (c) follows from $\langle \mathbf{x}, \mathbf{y} \rangle \leq \frac{1}{2} [\|\mathbf{x}\|^2 + \|\mathbf{y}\|^2]$; and (d) is due to the Cauchy-Schwartz inequality and **Assumption 1**.

The upper bound of $T_{2,2}$ is derived as

$$\begin{aligned}
T_{2,2} &\stackrel{(a)}{=} \left\langle \sqrt{c\eta U} \nabla f(\boldsymbol{\theta}^t), \mathbb{E} \left[\frac{\sqrt{c\eta}}{S\sqrt{U}} \sum_{m \in \mathcal{S}^t} \frac{\langle \mathbf{g}_m^t, \mathbf{r}^t \rangle}{\|\mathbf{g}_m^t\| \|\mathbf{r}^t\|} a_5 \right] \right\rangle \\
&\stackrel{(b)}{\leq} \frac{c\eta U}{2} \mathbb{E} [\|\nabla f(\boldsymbol{\theta}^t)\|^2] + \frac{c\eta}{S^2 U} \mathbb{E} \left[\left\| \sum_{m \in \mathcal{S}^t} \frac{\langle \mathbf{g}_m^t, \mathbf{r}^t \rangle}{\|\mathbf{g}_m^t\| \|\mathbf{r}^t\|} a_5 \right\|^2 \right] \\
&\stackrel{(c)}{\leq} \frac{c\eta U}{2} \mathbb{E} [\|\nabla f(\boldsymbol{\theta}^t)\|^2] + \frac{c\eta}{SU} \sum_{m \in \mathcal{S}^t} \mathbb{E} [\|a_5\|^2], \quad (30)
\end{aligned}$$

where $a_5 = \sum_{u=0}^{U-1} \nabla F_m(\boldsymbol{\theta}_m^{t,u})$; (a) is due to the definition of \mathbf{g}_m^t ; (b) follows from $\langle \mathbf{x}, \mathbf{y} \rangle \leq \frac{1}{2} [\|\mathbf{x}\|^2 + \|\mathbf{y}\|^2]$; and (c) is based on the Cauchy-Schwartz inequality and triangle inequality.

The upper bound of $T_{2,3}$ is given by

$$\begin{aligned}
T_{2,3} &= \left\langle \sqrt{c\eta U} \nabla f(\boldsymbol{\theta}^t), \mathbb{E} \left[\frac{\sqrt{c}}{S\sqrt{\eta U}} \sum_{m \in \mathcal{S}^t} \frac{\|\mathbf{g}_m^t\| \|\mathbf{r}^t\| - \langle \mathbf{g}_m^t, \mathbf{r}^t \rangle}{\|\mathbf{r}^t\|^2} \mathbf{r}^t \right] \right\rangle \\
&\stackrel{(a)}{\leq} \frac{c\eta U}{2} \mathbb{E} [\|\nabla f(\boldsymbol{\theta}^t)\|^2] \\
&+ \frac{c}{2\eta US^2} \mathbb{E} \left[\left\| \sum_{m \in \mathcal{S}^t} \frac{\|\mathbf{g}_m^t\| \|\mathbf{r}^t\| - \langle \mathbf{g}_m^t, \mathbf{r}^t \rangle}{\|\mathbf{r}^t\|^2} \right\|^2 \|\mathbf{r}^t\|^2 \right] \\
&\stackrel{(b)}{\leq} \frac{c\eta U}{2} \mathbb{E} [\|\nabla f(\boldsymbol{\theta}^t)\|^2] + \frac{c}{2\eta US^2} \mathbb{E} \left[\left(2 \sum_{m \in \mathcal{S}^t} \|\mathbf{g}_m^t\| \right)^2 \right] \\
&\stackrel{(c)}{\leq} \frac{c\eta U}{2} \mathbb{E} [\|\nabla f(\boldsymbol{\theta}^t)\|^2] + 2c\eta\sigma_L^2 + \frac{2c\eta}{MU} \sum_{m \in \mathcal{M}} \mathbb{E} [\|a_5\|^2], \quad (31)
\end{aligned}$$

where (a) comes from $\langle \mathbf{x}, \mathbf{y} \rangle \leq \frac{1}{2} [\|\mathbf{x}\|^2 + \|\mathbf{y}\|^2]$; (b) follows from the triangle inequality, and (c) is based on **Assumption 2** and uniform worker sampling without replacement.

We further bound $\mathbb{E} [\|a_5\|^2]$ in (30) and (31); i.e.,

$$\begin{aligned}
\mathbb{E} [\|a_5\|^2] &= \mathbb{E} \left[\left\| \sum_{u=0}^{U-1} (a_3 + \nabla F_m(\boldsymbol{\theta}^t) - \nabla f(\boldsymbol{\theta}^t) + \nabla f(\boldsymbol{\theta}^t)) \right\|^2 \right] \\
&\stackrel{(a)}{\leq} 3UL^2 \sum_{u=0}^{U-1} \mathbb{E} [\|\boldsymbol{\theta}_m^{t,u} - \boldsymbol{\theta}^t\|^2] + 3U^2\sigma_G^2 + 3U^2 \|\nabla f(\boldsymbol{\theta}^t)\|^2 \\
&\stackrel{(b)}{=} C_1 \mathbb{E} [\|\nabla f(\boldsymbol{\theta}^t)\|^2] + C_2, \quad (32)
\end{aligned}$$

where $C_1 = 90U^4L^2\eta^2 + 3U^2$; $C_2 = 15U^3L^2\eta^2(\sigma_L^2 + 6U\sigma_G^2) + 3U^2\sigma_G^2$; (a) is due to the Cauchy-Schwartz inequality; (b) is based on [40, Lemma 3], which yields: $\forall 1 \leq u \leq U$, $\mathbb{E} [\|\boldsymbol{\theta}_m^{t,u} - \boldsymbol{\theta}^t\|^2] \leq 5U\eta^2(\sigma_L^2 + 6U\sigma_G^2) + 30U^2\eta^2 \mathbb{E} [\|\nabla f(\boldsymbol{\theta}^t)\|^2]$.

Together with the upper bounds of T_1 , $T_{2,1}$, $T_{2,2}$ and $T_{2,3}$ in (27), (29), (30) and (31), respectively, we rewrite (26) as

$$\begin{aligned}
\mathbb{E} [f(\boldsymbol{\theta}^{t+1})] &\leq f(\boldsymbol{\theta}^t) - \eta U \left(\frac{1-3c}{2} - \left(\frac{3c}{U} + \frac{\eta L}{2} \right) (90U^3L^2\eta^2 + 3U) \right. \\
&\quad \left. - \frac{30(1-c)L^2U^2\eta^2}{2} \right) \mathbb{E} [\|\nabla f(\boldsymbol{\theta}^t)\|^2] + C_3, \quad (33)
\end{aligned}$$

where $C_3 = 2c\eta\sigma_L^2 + \frac{\eta^2 U\sigma_L^2 L}{2} + (\frac{3c\eta}{U} + \frac{\eta^2 L}{2})C_2 + \frac{5(1-c)\eta^3 L^2 U^2}{2}(\sigma_L^2 + 6U\sigma_G^2)$. With $\eta \leq \frac{1}{8LU}$, we can prove that there exists a positive constant γ satisfying

$$\gamma < \frac{1-3c}{2} - \left(\frac{3c}{U^2} + \frac{\eta L}{2U} \right) C_1 - \frac{30(1-c)L^2U^2\eta^2}{2}. \quad (34)$$

Rearranging (33) and summing from $t = 0, \dots, T-1$ yields

$$\frac{1}{T} \sum_{t=0}^{T-1} \mathbb{E} [\|\nabla f(\boldsymbol{\theta}^t)\|^2] \leq \frac{f(\boldsymbol{\theta}^0) - f^*}{\gamma\eta UT} + V, \quad (35)$$

where $V = \frac{C_3}{\gamma U \eta}$. The proof is complete.

APPENDIX B PROOF OF THEOREM 2

As with Appendix A, with the L -smoothness of f , we have

$$\begin{aligned}
\mathbb{E} [f(\boldsymbol{\theta}^{t+1})] &\leq f(\boldsymbol{\theta}^t) + \langle \nabla f(\boldsymbol{\theta}^t), \mathbb{E} [\boldsymbol{\theta}^{t+1} - \boldsymbol{\theta}^t] \rangle + \frac{L}{2} \mathbb{E} [\|\Delta^t\|^2] \\
&= f(\boldsymbol{\theta}^t) + T_1 + T_2 + \frac{L}{2} T_3, \quad (36)
\end{aligned}$$

where $T_1 = \mathbb{E} [\langle \nabla f(\boldsymbol{\theta}^t), \frac{1}{S} \sum_{m \in \mathcal{A}^t} \mathbf{v}_m^t \rangle]$, $T_2 = \mathbb{E} [\langle \nabla f(\boldsymbol{\theta}^t), \frac{1}{S} \sum_{m \in \mathcal{B}^t} \mathbf{v}_m^t \rangle]$, and $T_3 = \mathbb{E} [\|\Delta^t\|^2]$.

With the definition of \mathbf{v}_m^t in (15) and **Assumption 4**, the modified gradient \mathbf{v}_m^t can be rewritten as

$$\mathbf{v}_m^t = h_m^t \mathbf{r}^t + (1 - h_m^t) \|\mathbf{r}^t\| \frac{\mathbf{g}_m^t}{\|\mathbf{g}_m^t\|}, \quad \forall m \in \mathcal{A}^t, \quad (37)$$

where $h_m^t = c^t(1 - x_m^t)$. Then, T_1 can be upper bounded by

$$\begin{aligned}
T_1 &= \mathbb{E} \left[\left\langle \nabla f(\boldsymbol{\theta}^t), \frac{1}{S} \sum_{m \in \mathcal{A}^t} h_m^t \mathbf{r}^t + (1 - h_m^t) \|\mathbf{r}^t\| \frac{\mathbf{g}_m^t}{\|\mathbf{g}_m^t\|} \right\rangle \right] \\
&\stackrel{(a)}{=} -c^t(w^t - x^t) \eta U \|\nabla f(\boldsymbol{\theta}^t)\|^2 \\
&+ \mathbb{E} [\langle \nabla f(\boldsymbol{\theta}^t), c^t(w^t - x^t) \eta U \nabla f(\boldsymbol{\theta}^t) + c^t(w^t - x^t) \mathbf{r}^t \rangle] \\
&+ \mathbb{E} \left[\left\langle \nabla f(\boldsymbol{\theta}^t), \frac{1}{S} \sum_{m \in \mathcal{A}^t} (1 - h_m^t) \|\mathbf{r}^t\| \frac{\mathbf{g}_m^t}{\|\mathbf{g}_m^t\|} \right\rangle \right], \quad (38)
\end{aligned}$$

where (a) is due to $A^t = w^t S$.

For the malicious workers $m \in \mathcal{A}^t$, define $x_m^t = \frac{\langle \mathbf{g}_m^t, \mathbf{r}^t \rangle}{\|\mathbf{g}_m^t\| \|\mathbf{r}^t\|}$ and $x^t = \frac{1}{S} \sum_{m \in \mathcal{A}^t} x_m^t$. The second term on the RHS of (38) is upper bounded, as given by

$$\mathbb{E} [\langle \nabla f(\boldsymbol{\theta}^t), c^t(w^t - x^t) \eta U \nabla f(\boldsymbol{\theta}^t) + c^t(w^t - x^t) \mathbf{r}^t \rangle]$$

$$\begin{aligned}
&\stackrel{(a)}{=} \left\langle \sqrt{\delta^t} \nabla f(\boldsymbol{\theta}^t), \frac{\sqrt{\delta^t}}{U} \mathbb{E} \left[\sum_{u=0}^{U-1} \nabla f(\boldsymbol{\theta}^t) - \nabla f(\boldsymbol{\theta}^{t,u}) \right] \right\rangle \\
&\stackrel{(b)}{\leq} \frac{\delta^t}{2} \mathbb{E} \left[\|\nabla f(\boldsymbol{\theta}^t)\|^2 \right] + \frac{\delta^t L^2}{2U} \sum_{u=0}^{U-1} \mathbb{E} \left[\|\boldsymbol{\theta}^{t,u} - \boldsymbol{\theta}^t\|^2 \right]. \quad (39)
\end{aligned}$$

Here, $\delta^t = c^t(w^t - x^t)\eta U$. (a) follows from (13); (b) is due to $\langle \mathbf{x}, \mathbf{y} \rangle \leq \frac{1}{2} [\|\mathbf{x}\|^2 + \|\mathbf{y}\|^2]$ and **Assumption 1**.

The last term on the RHS of (38) is bounded as

$$\begin{aligned}
&\mathbb{E} \left[\left\langle \nabla f(\boldsymbol{\theta}^t), \frac{1}{S} \sum_{m \in \mathcal{A}^t} (1 - h_m^t) \|\mathbf{r}^t\| \frac{\mathbf{g}_m^t}{\|\mathbf{g}_m^t\|} \right\rangle \right] \\
&= \mathbb{E} \left[\left\langle \sqrt{\delta^t} \nabla f(\boldsymbol{\theta}^t), \frac{1}{S\sqrt{\delta^t}} \sum_{m \in \mathcal{A}^t} (1 - h_m^t) \|\mathbf{r}^t\| \frac{\mathbf{g}_m^t}{\|\mathbf{g}_m^t\|} \right\rangle \right] \\
&\stackrel{(a)}{\leq} \frac{\delta^t}{2} \mathbb{E} \left[\|\nabla f(\boldsymbol{\theta}^t)\|^2 \right] + \frac{\left\| \sum_{m \in \mathcal{A}^t} (1 - h_m^t) \right\|^2}{2S^2\delta^t} \mathbb{E} \left[\|\mathbf{r}^t\|^2 \right], \quad (40)
\end{aligned}$$

where (a) comes from $\langle \mathbf{x}, \mathbf{y} \rangle \leq \frac{1}{2} [\|\mathbf{x}\|^2 + \|\mathbf{y}\|^2]$.

Similarly, for the upper bound of T_2 , we have

$$\begin{aligned}
T_2 &= -c^t(1 - w^t - y^t)\eta U \mathbb{E} \left[\|\nabla f(\boldsymbol{\theta}^t)\|^2 \right] \\
&+ \mathbb{E} \left[\langle \nabla f(\boldsymbol{\theta}^t), c^t(1 - w^t - y^t)(\mathbf{r}^t + \eta U \nabla f(\boldsymbol{\theta}^t)) \rangle \right] \\
&+ \mathbb{E} \left[\left\langle \nabla f(\boldsymbol{\theta}^t), \frac{1}{S} \sum_{m \in \mathcal{B}^t} (1 - l_m^t) \rho_m^t \mathbf{g}_m^t \right\rangle \right], \quad (41)
\end{aligned}$$

where $l_m^t = c^t(1 - y_m^t)$ and $y^t = \frac{1}{S} \sum_{m \in \mathcal{B}^t} y_m^t$.

As with (39), with $\kappa^t = c^t(1 - w^t - y^t)\eta U$, the second term on the RHS of (41) can be bounded as

$$\begin{aligned}
&\mathbb{E} \left[\langle \nabla f(\boldsymbol{\theta}^t), c^t(1 - w^t - y^t)(\mathbf{r}^t + \eta U \nabla f(\boldsymbol{\theta}^t)) \rangle \right] \\
&\leq \frac{\kappa^t}{2} \mathbb{E} \left[\|\nabla f(\boldsymbol{\theta}^t)\|^2 \right] + \frac{\kappa^t L^2}{2U} \sum_{u=0}^{U-1} \mathbb{E} \left[\|\boldsymbol{\theta}^{t,u} - \boldsymbol{\theta}^t\|^2 \right], \quad (42)
\end{aligned}$$

based on the Cauchy-Schwarz inequality and **Assumption 1**.

The third term on the RHS of (41) is upper bounded as

$$\begin{aligned}
&\mathbb{E} \left[\left\langle \nabla f(\boldsymbol{\theta}^t), \frac{1}{S} \sum_{m \in \mathcal{B}^t} (1 - l_m^t) \rho_m^t \mathbf{g}_m^t \right\rangle \right] \\
&\stackrel{(a)}{=} \frac{-1}{b^t} \mathbb{E} \left[\left\langle b^t \nabla f(\boldsymbol{\theta}^t), \frac{1}{S} \sum_{m \in \mathcal{B}^t} b_m^t \sum_{u=0}^{U-1} \eta \nabla F_m(\boldsymbol{\theta}_m^{t,u}) \right\rangle \right] \\
&\stackrel{(b)}{\leq} \frac{-b^t \eta U}{2} \mathbb{E} \left[\|\nabla f(\boldsymbol{\theta}^t)\|^2 \right] \\
&+ \frac{1}{2b^t} \mathbb{E} \left[\left\| \frac{1}{S} \sum_{m \in \mathcal{B}^t} b_m^t \frac{\sqrt{\eta}}{\sqrt{U}} \sum_{u=0}^{U-1} \nabla F_m(\boldsymbol{\theta}^t) - \nabla F_m(\boldsymbol{\theta}_m^{t,u}) \right\|^2 \right] \\
&\stackrel{(c)}{\leq} \frac{\eta L^2}{2b^t S} \sum_{m \in \mathcal{B}^t} (b_m^t)^2 \sum_{u=0}^{U-1} \mathbb{E} \left[\|\boldsymbol{\theta}^t - \boldsymbol{\theta}_m^{t,u}\|^2 \right] - \frac{b^t \eta U}{2} \|\nabla f(\boldsymbol{\theta}^t)\|^2, \quad (43)
\end{aligned}$$

where $b_m^t = (1 - l_m^t) \rho_m^t$, and $b^t = \frac{1}{S} \sum_{m \in \mathcal{B}^t} b_m^t$; (a) is due to $\mathbf{g}_m^t = \boldsymbol{\theta}_m^{t,U} - \boldsymbol{\theta}^t$ and **Assumption 2**; (b) comes from $-2 \langle \mathbf{x}, \mathbf{y} \rangle \leq -\|\mathbf{x}\|^2 + \|\mathbf{x} - \mathbf{y}\|^2$; and (c) is due to **Assumption 1** and the Cauchy-Schwarz inequality.

By the triangle inequality, $\|\mathbf{v}_m^t\| \leq \|(1 - \lambda_m^t) \frac{\|\mathbf{r}^t\|}{\|\mathbf{g}_m^t\|} \mathbf{g}_m^t\| + \|\lambda_m^t \mathbf{r}^t\| \leq \|\mathbf{r}^t\|, \forall i \in \mathcal{S}^t$. Then, T_3 is upper bounded by

$$T_3 \stackrel{(a)}{\leq} \frac{1}{S} \sum_{m \in \mathcal{S}^t} \mathbb{E} \left[\|\mathbf{r}^t\|^2 \right] = \mathbb{E} \left[\|\mathbf{r}^t\|^2 \right], \quad (44)$$

where (a) is based on the Cauchy-Schwarz inequality.

By the definition of \mathbf{r}^t in (13), it follows that

$$\begin{aligned}
\mathbb{E} \left[\|\mathbf{r}^t\|^2 \right] &\stackrel{(a)}{\leq} \mathbb{E} \left[\|\boldsymbol{\theta}^{t,U-1} - \boldsymbol{\theta}^t - \eta \nabla f(\boldsymbol{\theta}^{t,U-1})\|^2 \right] + \eta^2 \sigma_L^2 \\
&\stackrel{(b)}{\leq} (1 + \frac{1}{2U-1}) \mathbb{E} \left[\|\boldsymbol{\theta}^{t,U-1} - \boldsymbol{\theta}^t\|^2 \right] + \eta^2 \sigma_L^2 \\
&+ 2\eta^2 U \mathbb{E} \left[\|\nabla f(\boldsymbol{\theta}^{t,U-1}) - \nabla f(\boldsymbol{\theta}^t) + \nabla f(\boldsymbol{\theta}^t)\|^2 \right] \\
&\stackrel{(c)}{\leq} (1 + \frac{1}{2U-1} + 4\eta^2 U L^2) \mathbb{E} \left[\|\boldsymbol{\theta}^{t,U-1} - \boldsymbol{\theta}^t\|^2 \right] \\
&+ 4\eta^2 U \mathbb{E} \left[\|\nabla f(\boldsymbol{\theta}^t)\|^2 \right] + \eta^2 \sigma_L^2 \\
&\stackrel{(d)}{\leq} \frac{U}{U-1} \mathbb{E} \left[\|\boldsymbol{\theta}^{t,U-1} - \boldsymbol{\theta}^t\|^2 \right] + 4\eta^2 U \mathbb{E} \left[\|\nabla f(\boldsymbol{\theta}^t)\|^2 \right] + \eta^2 \sigma_L^2 \\
&\stackrel{(e)}{\leq} 8\eta^2 U^2 \mathbb{E} \left[\|\nabla f(\boldsymbol{\theta}^t)\|^2 \right] + 2\eta^2 U \sigma_L^2, \quad (45)
\end{aligned}$$

where (a) is due to $\mathbb{E} [\|\mathbf{x}\|^2] = \mathbb{E} [\|\mathbf{x} - \mathbb{E}[\mathbf{x}]\|^2 + \|\mathbb{E}[\mathbf{x}]\|^2]$ and **Assumption 2**; (b) comes from Young's inequality; (c) is based on the Cauchy-Schwarz inequality and **Assumption 1**; (d) holds since $\frac{1}{2U-1} + 4\eta^2 U L^2 \leq \frac{1}{U-1}$ with $\eta \leq \frac{1}{3UL}$; and (e) is due to $(1 + \frac{1}{U-1})^U \leq 2U$. It can also be verified that (45) holds when $U = 1$. For $1 \leq u \leq U$, we now have

$$\mathbb{E} \left[\|\boldsymbol{\theta}^{t,u} - \boldsymbol{\theta}^t\|^2 \right] \leq 8\eta^2 U^2 \mathbb{E} \left[\|\nabla f(\boldsymbol{\theta}^t)\|^2 \right] + 2\eta^2 U \sigma_L^2. \quad (46)$$

Together with the upper bounds of T_1 , T_2 , and T_3 based on (39), (40), (42), (43) and (46), we can rewrite (36) as

$$\mathbb{E} [f(\boldsymbol{\theta}^{t+1})] \leq f(\boldsymbol{\theta}^t) - \eta U D_1^t \mathbb{E} \left[\|\nabla f(\boldsymbol{\theta}^t)\|^2 \right] + D_2^t, \quad (47)$$

where $D_1^t = \frac{\kappa^t}{2\eta U} + \frac{b^t}{2} - 8\eta U - 4(\delta^t + \kappa^t)\eta U L^2 - \frac{4\eta^2 U^2 L^2}{b^t S} \sum_{m \in \mathcal{B}^t} (b_m^t)^2 - 4\eta U \frac{\|\sum_{m \in \mathcal{A}^t} (1 - h_m^t)\|^2}{S^2 \delta^t}$, and $D_2^t = 2\eta^2 U \sigma_L^2 \left(\frac{(\delta^t + \kappa^t)L^2}{2} + \frac{\|\sum_{m \in \mathcal{A}^t} (1 - h_m^t)\|^2}{2S^2 \delta^t} \right) + \frac{\eta U L^2}{2b^t S} \sum_{m \in \mathcal{B}^t} (b_m^t)^2 + 1$.

Since the malicious workers can potentially upload any local updates, we have $x^t \in [-w^t, w^t]$ and $\delta^t \in (0, 2c^t w^t \eta U]$. Hence, $y^t \in (0, 1 - w^t]$, $(b_m^t)^2 \in [0, q^2]$, $b^t \in [(1 - w^t)(1 - c^t)p, (1 - w^t)q]$, and $\kappa^t \in [0, c^t(1 - w^t)\eta U]$ under **Assumptions 3** and **4**. Note that $\|\sum_{m \in \mathcal{A}^t} (1 - h_m^t)\|^2 = 0, \forall t$, when $c^t = \frac{w^t}{w^t - x^t} \in [\frac{1}{2}, 1]$. With the stepsize $\eta \leq \frac{(1-w^t)(1-c^t)p}{32U+2UL^2(p+2q^2)}, \forall t$, and the above ranges of δ^t , κ^t , b^t and b_m^t , we can prove that there is a positive constant χ^t satisfying

$$\begin{aligned}
\chi^t &< \frac{(1 - w^t)(1 - c^t)p}{2} - 8\eta U - \frac{4\eta^2 U^2 L^2}{(1 - c^t)p} q^2 \\
&- 4c^t(1 + w^t)L^2 \eta^2 U^2 < D_1^t, \quad \forall t, \quad (48)
\end{aligned}$$

Similarly, D_2^t can be upper bounded as

$$D_2^t \leq 2\eta^2 U \sigma_L^2 \left(\frac{(1+w^t)c^t\eta U L^2}{2} + \frac{\eta U L^2 q^2}{2(1-c^t)p} + 1 \right). \quad (49)$$

Define $\chi = \max_t \chi^t$, $D_2 = \max_t D_2^t$, $\tilde{c} = \max_t c^t$ and $\tilde{w} = \max_t w^t$. By reorganizing (47) and summing it over $t = 0, \dots, T-1$, we finally obtain

$$\frac{1}{T} \sum_{t=0}^{T-1} \mathbb{E} \left[\|\nabla f(\boldsymbol{\theta}^t)\|^2 \right] \leq \frac{f(\boldsymbol{\theta}^0) - f^*}{\chi \eta U T} + W. \quad (50)$$

Here, $\eta \leq \frac{(1-\bar{w})(1-\bar{c})p}{32U+2UL^2(p+2q^2)}$; $W = \frac{D_2}{\chi\eta U}$.

Since the PS may be unaware of the malicious workers, $c^t = \frac{w^t}{w^t-x^t}$ may not hold. Nevertheless, with the stepsize $\eta \leq \frac{2c^t(1-c^t)(1-w^t)(1-w^t-y^t)p}{32pU+c^tUL^2(p^2+q^2)}$, $\forall t$, if c^t satisfies

$$((\rho^t)^2 - 7w^t + 8x^t - 1)(c^t)^2 + (15w^t + 1)c^t \geq \frac{8(w^t)^2}{w^t - x^t}, \quad (51)$$

we can prove that there also exists a positive constant $\chi^t \leq D_1^t$, and D_2^t can be upper bounded as

$$D_2^t \leq 2\eta^2 U \sigma_L^2 \left(\frac{(1+w^t)c^t\eta UL^2}{2} + \frac{\eta UL^2 q^2}{2(1-c^t)p} + H^t + 1 \right), \quad (52)$$

where $H^t = \frac{\|\sum_{m \in \mathcal{A}^t} (1-h_m^t)\|^2}{2S^2\delta^t}$ is bounded. Then, (50) can also be attained. This proof concludes.

REFERENCES

- [1] B. McMahan, E. Moore, D. Ramage, S. Hampson, and B. A. y. Arcas, “Communication-efficient learning of deep networks from decentralized data,” in *Proc. Int. Conf. Artif. Intell. Stat. (AISTATS)*, vol. 54. PMLR, 2017, pp. 1273–1282.
- [2] K. Wei, J. Li, M. Ding, C. Ma, H. H. Yang, F. Farokhi, S. Jin, T. Q. S. Quek, and H. Vincent Poor, “Federated learning with differential privacy: Algorithms and performance analysis,” *IEEE Trans. Inf. Forensics Secur.*, vol. 15, pp. 3454–3469, 2020.
- [3] Y. Zhao, M. Li, L. Lai, N. Suda, D. Civin, and V. Chandra, “Federated learning with non-iid data,” arXiv preprint arXiv:1806.00582, 2018.
- [4] J. So, B. Güler, and A. S. Avestimehr, “Byzantine-resilient secure federated learning,” *IEEE J. Sel. Areas Commun.*, vol. 39, no. 7, pp. 2168–2181, 2020.
- [5] A. Yazdinejad, A. Dehghantanha, H. Karimipour, G. Srivastava, and R. M. Parizi, “A robust privacy-preserving federated learning model against model poisoning attacks,” *IEEE Trans. Inf. Forensics Secur.*, vol. 19, pp. 6693–6708, 2024.
- [6] X. Li, K. Huang, W. Yang, S. Wang, and Z. Zhang, “On the convergence of FedAvg on non-iid data,” in *Proc. Int. Conf. Learn. Representations (ICLR)*, 2020.
- [7] G. Malinovskiy, D. Kovalev, E. Gasanov, L. Condat, and P. Richtarik, “From local SGD to local fixed-point methods for federated learning,” in *Proc. Int. Conf. Mach. Learn. (ICML)*, 2020, pp. 6692–6701.
- [8] A. Defazio, F. Bach, and S. Lacoste-Julien, “SAGA: A fast incremental gradient method with support for non-strongly convex composite objectives,” in *Proc. Neural Inf. Process. Syst. (NeurIPS)*, vol. 27, 2014.
- [9] X. Liang, S. Shen, J. Liu, Z. Pan, E. Chen, and Y. Cheng, “Variance reduced local SGD with lower communication complexity,” arXiv preprint arXiv:1912.12844, 2019.
- [10] T. Li, A. K. Sahu, M. Zaheer, M. Sanjabi, A. Talwalkar, and V. Smithy, “FedDANE: A federated Newton-type method,” in *Proc. Asilomar Conf. Signals, Syst., and Comput.*, 2019, pp. 1227–1231.
- [11] R. Pathak and M. J. Wainwright, “FedSplit: An algorithmic framework for fast federated optimization,” in *Proc. Neural Inf. Process. Syst. (NeurIPS)*, vol. 33, 2020, pp. 7057–7066.
- [12] A. Mitra, R. Jaafar, G. J. Pappas, and H. Hassani, “Linear convergence in federated learning: Tackling client heterogeneity and sparse gradients,” in *Proc. Neural Inf. Process. Syst. (NeurIPS)*, vol. 34, 2021, pp. 14 606–14 619.
- [13] S. P. Karimireddy, S. Kale, M. Mohri, S. Reddi, S. Stich, and A. T. Suresh, “SCAFFOLD: Stochastic controlled averaging for federated learning,” in *Proc. Int. Conf. Mach. Learn. (ICML)*, 2020, pp. 5132–5143.
- [14] D. A. E. Acar, Y. Zhao, R. Matas, M. Mattina, P. Whatmough, and V. Saligrama, “Federated learning based on dynamic regularization,” in *Proc. Int. Conf. Learn. Representations (ICLR)*, 2021.
- [15] S. P. Karimireddy, M. Jaggi, S. Kale, M. Mohri, S. J. Reddi, S. U. Stich, and A. T. Suresh, “MIME: Mimicking centralized stochastic algorithms in federated learning,” arXiv preprint arXiv:2008.03606, 2020.
- [16] T. Li, A. K. Sahu, M. Zaheer, M. Sanjabi, A. Talwalkar, and V. Smith, “Federated optimization in heterogeneous networks,” in *Proc. Mach. Learn. Syst. (MLSys)*, vol. 2, 2020, pp. 429–450.
- [17] L. Gao, H. Fu, L. Li, Y. Chen, M. Xu, and C.-Z. Xu, “FedDC: Federated learning with non-iid data via local drift decoupling and correction,” in *Proc. IEEE/CVF Conf. Comput. Vis. Pattern Recognit. (CVPR)*, 2022, pp. 10 112–10 121.
- [18] Z. Qu, X. Li, R. Duan, Y. Liu, B. Tang, and Z. Lu, “Generalized federated learning via sharpness aware minimization,” in *Proc. Int. Conf. Mach. Learn. (ICML)*, vol. 162. PMLR, 17–23 Jul 2022, pp. 18 250–18 280.
- [19] B. Li and G. Giannakis, “Enhancing sharpness-aware optimization through variance suppression,” in *Proc. Neural Inf. Process. Syst. (NeurIPS)*, vol. 36, 2023, pp. 70 861–70 879.
- [20] D. Jhunjhunwala, S. Wang, and G. Joshi, “FedExP: Speeding up federated averaging via extrapolation,” in *Proc. Int. Conf. Learn. Representations (ICLR)*, 2023.
- [21] G. Kim, J. Kim, and B. Han, “Communication-efficient federated learning with accelerated client gradient,” in *Proc. IEEE/CVF Conf. Comput. Vis. Pattern Recognit. (CVPR)*, June 2024, pp. 12 385–12 394.
- [22] Z. Zhang, L. Wu, C. Ma, J. Li, J. Wang, Q. Wang, and S. Yu, “LSFL: A lightweight and secure federated learning scheme for edge computing,” *IEEE Trans. Inf. Forensics Secur.*, vol. 18, pp. 365–379, 2023.
- [23] S. Li, E. Ngai, and T. Voigt, “Byzantine-robust aggregation in federated learning empowered industrial IoT,” *IEEE Trans. Ind. Informat.*, vol. 19, no. 2, pp. 1165–1175, 2023.
- [24] L. Li, W. Xu, T. Chen, G. B. Giannakis, and Q. Ling, “RSA: Byzantine-robust stochastic aggregation methods for distributed learning from heterogeneous datasets,” in *Proc. Conf. Artif. Intell. (AAAI)*, vol. 33, no. 01, 2019, pp. 1544–1551.
- [25] Y. Jiang, W. Zhang, and Y. Chen, “Data quality detection mechanism against label flipping attacks in federated learning,” *IEEE Trans. Inf. Forensics Secur.*, vol. 18, pp. 1625–1637, 2023.
- [26] P. Blanchard, E. M. El Mhamdi, R. Guerraoui, and J. Stainer, “Machine learning with adversaries: Byzantine tolerant gradient descent,” in *Proc. Neural Inf. Process. Syst. (NeurIPS)*, vol. 30, 2017.
- [27] M. Fang, X. Cao, J. Jia, and N. Gong, “Local model poisoning attacks to Byzantine-robust federated learning,” in *Proc. USENIX Secur. Symp. (USENIX Secur.)*, 2020, pp. 1605–1622.
- [28] D. Yin, Y. Chen, R. Kannan, and P. Bartlett, “Byzantine-robust distributed learning: Towards optimal statistical rates,” in *Proc. Int. Conf. Mach. Learn. (ICML)*, 2018, pp. 5650–5659.
- [29] X. Cao, M. Fang, J. Liu, and N. Z. Gong, “FLTrust: Byzantine-robust federated learning via trust bootstrapping,” in *Proc. Netw. Distrib. Syst. Secur. Symp. (NDSS)*, 2020, pp. 2938–2948.
- [30] K. Pillutla, S. M. Kakade, and Z. Harchaoui, “Robust aggregation for federated learning,” *IEEE Trans. Signal Process.*, vol. 70, pp. 1142–1154, 2022.
- [31] S. MINSKER, “Geometric median and robust estimation in banach spaces,” *Bernoulli*, vol. 21, no. 4, pp. 2308–2335, 2015.
- [32] Z. Wu, Q. Ling, T. Chen, and G. B. Giannakis, “Federated variance-reduced stochastic gradient descent with robustness to Byzantine attacks,” *IEEE Trans. Signal Process.*, vol. 68, pp. 4583–4596, 2020.
- [33] H. Zhu and Q. Ling, “Byzantine-robust distributed learning with compression,” *IEEE Trans. Signal Inf. Process. Networks*, vol. 9, pp. 280–294, 2023.
- [34] S. Zuo, X. Yan, R. Fan, H. Hu, H. Shan, and T. Q. Quek, “Byzantine-resilient federated learning with adaptivity to data heterogeneity,” arXiv preprint arXiv:2403.13374, 2024.
- [35] C. Northcutt, L. Jiang, and I. Chuang, “Confident learning: Estimating uncertainty in dataset labels,” *J. Artif. Intell. Res.*, vol. 70, pp. 1373–1411, 2021.
- [36] F. Kato, Y. Cao, and M. Yoshikawa, “Olive: Oblivious federated learning on trusted execution environment against the risk of sparsification,” *Proc. VLDB Endow.*, vol. 16, no. 10, p. 2404–2417, Jun. 2023.
- [37] G. Cohen, S. Afshar, J. Tapson, and A. Van Schaik, “EMNIST: Extending MNIST to handwritten letters,” in *Proc. Int. Joint Conf. Neural Netw. (IJCNN)*, 2017, pp. 2921–2926.
- [38] A. Krizhevsky and G. Hinton, “Learning multiple layers of features from tiny images,” 2009.
- [39] A. Beck and S. Sabach, “Weiszfeld’s method: Old and new results,” *J. Optim. Theory Appl.*, vol. 164, no. 1, pp. 1–40, 2015.
- [40] S. J. Reddi, Z. Charles, M. Zaheer, Z. Garrett, K. Rush, J. Konečný, S. Kumar, and H. B. McMahan, “Adaptive federated optimization,” in *Proc. Int. Conf. Learn. Representations (ICLR)*, 2021.